Synoptic Scale Weather Patterns Associated with Annual Snow Accumulation Variability in North-Central Greenland

By

Shu Chen

Submitted to the graduate degree program in Geography and the Graduate Faculty of the University of Kansas in partial fulfillment of the requirements for the degree of Master of Science.

_____

Chairperson David Braaten

_____

David Mechem

_____

Donna Tucker

Date Defended: 6 February 2013

The Thesis Committee for Shu Chen

certifies that this is the approved version of the following thesis:

Synoptic Scale Weather Patterns Associated with Annual Snow Accumulation Variability in North-Central Greenland

_____

Chairperson David Braaten

Date approved: 24 May 2013

Abstract

Previous studies on the synoptic forcing of high elevation areas of central Greenland have mostly relied on ice cores, snow pits, mesoscale models, and climate models. In this study, a radar-measured 118-year annual snow accumulation record (1889-2006) along a 375 km traverse between NGRIP and NEEM ice camps in Greenland is used. A Self-Organizing Maps (SOM) algorithm is applied to a reanalysis forecast model (20th Century Reanalysis Data Version 2 (1870 to 2008)) to identify recurring patterns in the sea level pressure (SLP) field that impact meteorological processes and explain annual variations of accumulation over North-Central Greenland for the 118 year period.

The SOM algorithm identified 36 representative daily SLP patterns over the North Atlantic region. Synoptic weather patterns shown in these SLP patterns include cyclone splitting, cyclone-blocking, and cyclone tracks indicating changes in cyclone position and cyclone intensity. Based on radar-measured annual snow accumulation, common SLP patterns for wet years (more accumulation) over North-Central Greenland are characterized by low pressure systems surrounding Greenland or cyclones approaching the west coast of Greenland, conveying moisture through a topographically lifted onshore flow; these patterns are mostly associated with negative/neutral NAO index. In dry years (less accumulation), prevailing patterns are characterized by cyclones positioned a long distance away in the Atlantic Ocean south of Greenland, which are mainly associated with a positive NAO index. Extreme wet year prevailing patterns of NGRIP-NEEM traverse southern portion show a distinct departure from the above described North-Central Greenland general patterns by having more frequent positive-NAO days, which is similar to dry and extreme dry years. Model precipitation amounts over North-Central Greenland from the 20th Century Reanalysis Data are found to be overestimated by up to 10 cm/year.

Acknowledgements

I would like to acknowledge my advisor, David Braaten for patiently guiding my through this research. I would also like to thank David Mechem and Donna Tucker for serving on my thesis committee and providing many insightful inputs. Thank you to the Center for Remote Sensing of Ice Sheet (CReSIS), University of Kansas for providing me the research assistantship. I appreciate the support of the US National Science Foundation through grants ANT-0632321 and ANT-0424589.

The NEEM Traverse and Survey accumulation data used in this thesis is collected and processed by Hilary Barbour, Claude Laird, and Anthony Hoch from CReSIS and Susanne Buchardt from the Center for Ice and Climate, University of Copenhagen. The Twentieth Century Reanalysis V2 data is provided by the NOAA/OAR/ESRL PSD, Boulder, Colorado, USA, from their Web site at http://www.esrl.noaa.gov/psd. Support for the Twentieth Century Reanalysis Project dataset is provided by the U.S. Department of Energy, Office of Science Innovative and Novel Computational Impact on Theory and Experiment (DOE INCITE) program, and Office of Biological and Environmental Research (BER), and by the National Oceanic and Atmospheric Administration Climate Program Office.

Lastly, I would like to acknowledge my parents in Nanjing, Xing Chen and Xiaolei Ye, who have played a large role in supporting and encouraging me throughout these years.

Table of contents

Chapter 1 Introduction

Greenland has a surface area of over 2×10^6 km^2, of which more than 80% is covered by inland ice, known as the Greenland Ice Sheet (GrIS) (Bamber et al. 2001). It is estimated that complete melting of GrIS could cause global sea level to rise as much as 7.2 meters (23.6 feet) (Church et al. 2001). Since the 1880s, average global temperature has increased by approximately 0. 8 °C (Hansen et al. 2010); meanwhile, average temperatures over Greenland have increased by more than twice this number (Vinther et al. 2006). The UN Intergovernmental Panel on Climate Change (IPCC) predicts that warming in the Arctic will range from 2 to 9 °C by 2100, with winters warming more significantly than summers (IPCC, 2007).

Recent changes in the ice sheet suggest that it is already responding dramatically to this warming climate. Alley et al. (2007) discovered an overall net loss of mass caused by increased melting and ice discharge resulting in a loss of mass has very likely already contributed to sea level rise. It is estimated that GrIS losses 160 ± 50 Gt per year, corresponding to about 0.5 mm per year of sea level rise (SWIPA, 2009). Besides ice discharge at the margins and melting in the ablation zones, a recent thickening in the interior of the ice sheet was also identified, which is said to be a result of increased precipitation associated with recent negative/neutral NAO values (Johannessen et al., 2005; Thomas et al., 2006; Alley et al., 2007).

The vast interior of the GrIS has the highest elevation (> 3000 meters) and lies within the dry-snow zone (Benson et al. 1962, Fahnestock et al. 1993; Hall et al. 2006). The dry-snow zone is defined as a portion of the glacier where almost no surface melting takes place, and is surrounded by the percolation zone at lower elevations where surface melt occurs during the warm season and water percolates into the glacier, but does not reach the base of the glacier. In the dry-snow zone, percolation and soaking are negligible (Benson et al. 1962). Near-surface internal ice layers in the dry snow zone provide a means of assessing annual accumulation inputs to the ice sheet. These mass inputs to the ice sheet are dominated by episodic snowfall events that are strongly influenced by synoptic scale forcing.

The goal of this study is to examine past synoptic scale weather patterns from forecast model reanalysis by classifying the patterns using a Self-Organizing Maps (SOM) algorithm to answer the following questions:

1. What are the major storm tracks and cyclone activities of North Atlantic region present in the 20th Century Reanalysis Data, Version 2 (20CRv2)?

2. What synoptic patterns are responsible for precipitation over North-central Greenland based on 20CRv2 and annual accumulation data from a NGRIP-NEEM radar survey?

3. Are there differences in synoptic scale patterns during wet years and dry years in North-central Greenland? If the answer is positive, what are the prevailing synoptic patterns in each of these two types of years?

4. How are the North Atlantic Oscillation (NAO) and the Northern Annular Mode (NAM) related with the identified synoptic patterns?

5. How does long-term variability of North-central Greenland precipitation/annual accumulation compare with NAO and NAM records?

Answers to the questions raised above are studied, discussed and answered in the following chapters.

Chapter 2 Background

2.1 GRIS Physical Processes

When the climate is cold enough for snow to accumulate, an ice sheet starts to form. Through tens of thousands of years, the weight of new input from precipitation continuously compresses existing annual snow layers, forming annual ice layers. Ice sheets are also constantly spreading out due to their own weight, from the areas with high accumulation rates to the melting zones on the flanks. In coastal regions, ice is lost through surface melt and ice discharge; discharged ice could break off to form icebergs that eventually melt.

Precipitation is the main input source term for the ice sheet; evaporation, sublimation, melt, and ice discharge from glaciers are the main loss terms**.** When the input terms are less than the loss terms over time, the total mass of the ice sheet will gradually decrease. A study (SWIPA, 2009) of over 400,000 years of global sea level data and global temperature data shows a clear association between periods of lower and higher global temperature and changes in the size of the Greenland Ice Sheet. Fluctuations in the volume (size) of the ice sheet are also strongly anti-correlated with changes in sea level: growth of an ice sheet leads to falling of sea level falls, and vice versa. Moreover, increased Greenland Ice Sheet melt and freshwater input into the northern North Atlantic Ocean can weaken or even disrupt the global thermohaline

circulation and thus impact global climate (SWIPA, 2009).

The Greenland Ice Sheet is highly susceptible to a variety of meteorological forcing factors. Solid precipitation is the primary component of mass balance input; other input processes include snow drifted from elsewhere, retained rainwater, riming of fog droplets, and deposition of water vapor onto the snow as frost. Most precipitation (roughly 96%) that falls onto the ice sheet is snow; the remainder falls as rain near the ice sheet margins (SWIPA, 2009). Better understanding of mechanisms leading to precipitation and snow accumulation over Greenland is important for understanding causes of recent mass balance changes to the Greenland Ice Sheet as well as predicting future changes.

In the past, the Greenland Ice Sheet accumulation rate estimates have relied heavily on multi-year climatologies derived from ice cores, snow pits, and coastal precipitation records (Benson, 1962; Ohmura and Reeh, 1991; Ohmura et al., 1999). Accumulation records derived from stratigraphic layers and chemical records in ice cores and snow pits are prone to uncertainties caused by redistribution, erosion, and disturbance of wind (Anklin et al., 1998; Mosley-Thompson et al., 2001). In addition, previous studies have mentioned that these point measurements can only be used to estimate ice accumulations within a range of 150-200 km (Bales et al., 2001; McConnell et al., 2001). The lack of accuracy and spatial coverage in the inland areas has also led to poorly quantified uncertainty in these regions. Coastal precipitation data measures solid precipitation near the coast of Greenland; however, there still lacks straight-forward relation between these precipitation records and ice sheet's accumulation in the interior.

Meteorologists have applied General Circulation Models (GCM) (Ohmura et al., 1996; Thompson and Pollard, 1997; Glover,1999; Murphy et al., 2002), regional climate models (RCM) (Dethloff et al., 2002; Box et al., 2004, 2005, 2006; Fettweis et al., 2008; Ettema et al., 2009) and climate reanalysis data (Hanna et al., 2005, 2006, 2008) to the estimation of GrIS accumulation rates and ice sheet mass balance, improving temporal resolution and providing continuous spatial coverage. In situ data, including ice/firn core records, snow pits, and Automatic Weather Station (AWS) data, provide the means to assess and calibrate results from RCMs and GCMs. Box et al. (2006) characterized GrIS Surface Mass Balance (SMB) regional patterns over 1988 to 2004 using a Polar MM5 (Fifth Generation Mesoscale Model modified for polar climates), a regional climate data assimilation and downscaling model. Burgess et al. (2009) presented a more improved GrIS accumulation grid by compensating spatially varying bias in Polar MM5 solid precipitation, using firn/ice core and coastal stations/data as comparison (Fig. 1). They estimate an average accumulation rate of 339 mm/year water equivalent (w.e.; the amount of water contained within the ice layer, measured by the depth of water that would theoretically result if melted ice layer instantaneously) or 591 Gt/year for the period of 1957 to 2008, a value higher than previous studies by 75 to 104 Gt/year. The general spatial variability of GrIS accumulation agrees with previous studies (Calanca et al., 2000; Dethloff et al., 2002; Box et al., 2006; Burgess et al., 2009), including maximum accumulation along the southeast coast, large accumulations at the southern tip and along the west coast, moderate amount of accumulation in the interior of southern Greenland, and low accumulation in the vast north-central Greenland. Burgess et al.'s calibrated model identified 31% of GrIS's accumulation took place over the southeast,

which is a magnitude large enough to affect the overall GrIS surface mass balance during certain periods.

No long-term significant ice-sheet-wide accumulation trend was found. However, during 1960 to 1972, an accumulation increase in the west and decrease in the east occurred simultaneously (Burgess et al., 2006). Box et al., (2006) found an over-all positive but insignificant increasing trend during 1988 to 2004. Burgess et al. suggested that prior to 1992, the western ice sheet accumulation rate increased while the southeast accumulation rate slightly decreased, which agrees with results from the 40-Year ECMWF Re-Analysis (ERA-40) showing increasing precipitation during the 1990s (Hanna et al., 2005).

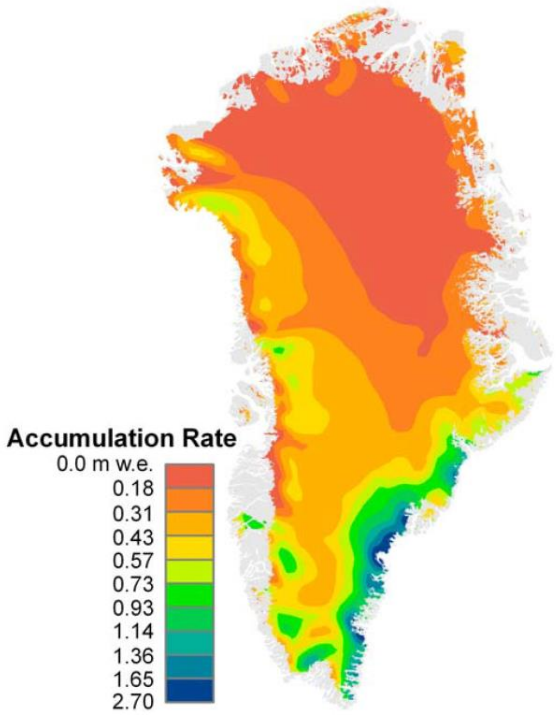

Fig. 1 Calibrated Polar MM5 annual accumulation rate map for 1958-2007 (Burgess et al. 2009)

2.2 Meteorological Forcing Factors

Precipitation over Greenland varies spatially. Bromwich et al. (1993) modeled the temporal and spatial properties of Greenland's precipitation for 1963 to 1988 from National Meteorological Center (NWC)'s geopotential heights data. Schunemann et al. (2009) estimated annual mean precipitation of the North Atlantic region during 1961 to 1999. Along with results from many other previous studies (Ohmura and Reeh 1991; Chen et al. 1997; Ohmura et al. 1999; Bales et al. 2001; Box et al., 2004, 2005, 2006),

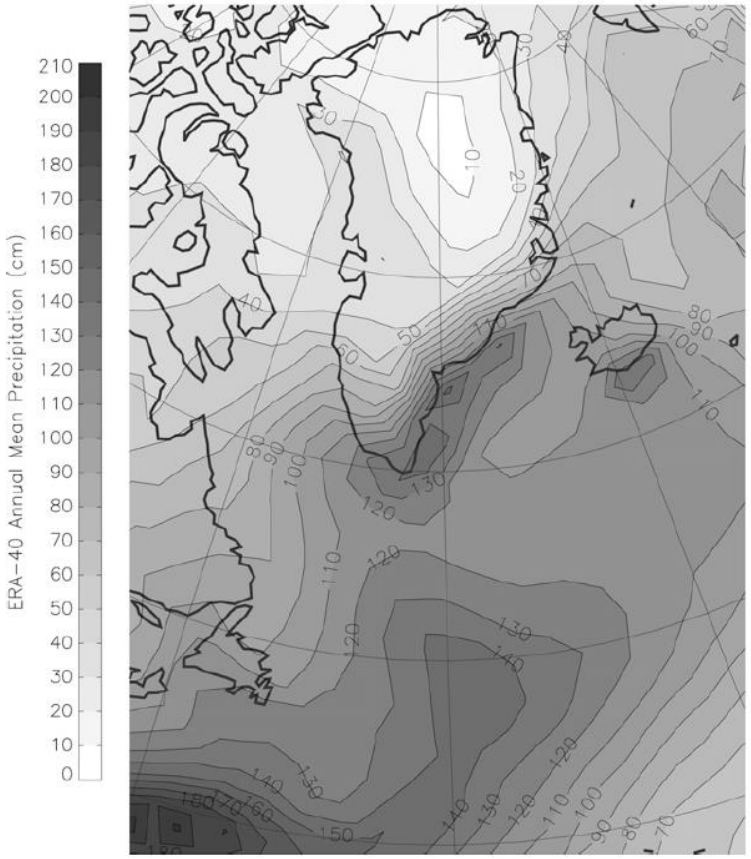

Fig. 2 Annual mean precipitation (cm) derived from ERA-40 (1961-1999) over the North Atlantic region. Contour interval is 10 cm. (Schuenemann et al., 2009)

there was agreement on similar spatial precipitation patterns: the southeast coast receives maximum precipitation of more than 165 cm/year; large magnitude of precipitation of

more than 100 cm/year falls over the southwest coast; western Greenland receives moderate amount of precipitation (> 50 cm/year); and low precipitation of less than 10 cm/year falls in the elevated area in north-central interior of Greenland. Overall, Schunamann et al. (2009) estimates 35.8 cm/year of mean precipitation over Greenland (Fig. 2), while Bromwich et al. (1998) obtained a value of 35.0 cm/year; later results all came close to this value (Ohmura et al. 1999; Bales et al. 2001; Box et al. 2004, 2005, 2006).

Precipitation patterns can generally be well explained by synoptic scale circulation patterns at the surface. The North Atlantic Storm Track and cyclones over the North Atlantic Region dominate Greenland's precipitation: interactions between cyclonic forcing, onshore flow, and Greenland's topographic features lead to most precipitation over Greenland (Chen et al. 1997). Chen et al. (1997) divided Greenland into 5 sub-regions according to their different precipitation characteristics. Over the northern coastal region and central inland region, summer precipitation is notably higher than other seasons. For central-west, central-east, and southern regions, clear relationships between precipitation and cyclonic activity were also found. Higher monthly mean frequency of Labrador Sea cyclones were linked to more precipitation over Greenland during certain months; frequent Icelandic cyclones were found to reduce precipitation over Greenland. Schunemann et al. (2009) also divided Greenland into five sub-regions (different from Chen et al.'s regions). Using ERA-40 daily resolved sea level pressure (SLP) data and a Self-Organizing Maps (SOM) algorithm, he identified three common storm tracks: blocking, splitting, and re-intensification of cyclones due to high elevations of the Greenland ice sheet. It is also found that when lows are situated in the Labrador Sea west

of Greenland or when a broad area of low pressure is surrounding Greenland, higher amounts of precipitation fall in western as well as central regions. Through a case study, Moore and Vachon (2002) identified that cyclone-splitting followed by re-intensification of secondary cyclone in the Labrador Sea is a potential genesis mechanism for polar lows. Polar lows are defined as fairly intense mesoscale cyclones (200km – 1000km in horizontal scale) that primarily develop during colder seasons in high latitude open seas (Rasmussen and Turner, 2003); they are common over the Norwegian Sea (Harley, 1960; Harrold and Browning, 1969) as well as in the Labrador Sea (Mailhot et al., 1996; Moore et al., 1996; Moore and Vachon, 2002). In summary, the greatest precipitation of each sub-region is caused by moist air transport by onshore and upslope flow.

A climatic seesaw effect negatively correlating with the wintertime climate of western Greenland and Northern Europe was discovered centuries ago and studied by many (Rogers and van Loon, 1979). The North Atlantic Oscillation (NAO) and the Northern Annular Mode (NAM, or Arctic Oscillation) are well known indices that help explain these teleconnection patterns, as well as other extratropical circulation patterns effecting climate patterns of the North Atlantic region. The NAO is a climatic index defined by the difference of atmospheric pressure at sea level between the Icelandic low and the Azores high that can have an influence on Greenland snow accumulation (Hurrell et al., 2003, 2009). The NAM, defined as the first Empirical Orthogonal Function (EOF) of winter Sea Level Pressure (SLP) data within the latitude range of 20°N to 90°N, is a good indicator of extended winter-mean (DJFM) variance. Previous studies found the NAO to causes the North Atlantic jet stream and some related storm tracks to change directions and intensity, with its resulting influence varying spatially and temporally

(Mosley-Thompson et al., 2005). Rogers and van Loon (1979) and Bromwich et al. (1999) revealed that a positive NAO scenario is associated with stronger westerlies and reduced southwesterly flow that brings moisture to Greenland, resulting in an overall average reduction of accumulation. Contrarily, with a negative NAO, the large-scale atmospheric flow is more frequently from the southwest, bringing more moisture to the ice sheets, particularly the south part of GRIS. Studies have claimed that the NAM and NAO maybe indistinguishable (Feldstein and Franzke, 2006), or indistinguishable at least during winter months (Rogers and McHugh, 2002). However, compared to the NAO index, the NAM provides an additional view on long-term synoptic patterns of the Arctic region, which may also play role in precipitation of Greenland.

Appenzeller et al. (1998) found a negative correlation between ice-core-based accumulation records of Western Greenland and NAO index during 1979 to 1993. Mosley-Thompson et al. (2005) studied the regional sensitivity of Greenland precipitation to NAO variability using PARCA (Program for Regional Climate Assessment) ice core data and inland core data (GITS, NASA-U, D2, D3, Summit, D1, and Raven). They found that accumulation at Summit (72°36’ N, 38°25’W) and Raven (66°29’ N, 46°18’ W), which are located in the central and southern-central, respectively, are poorly correlated to annual NAO index; whereas cores (GITS, NASA-U and D2) located in the west show a stronger negative correlation. It is also found that some of the cores from west Greenland exhibited a significant correlation with NAO before the 1920s warming, but faded afterwards. Banta and McConnell (2007) obtained similar results using records from four new ice cores, D4 and D5 in the central western Greenland, Sandy and Katie at Summit. For the Summit region (Sandy, Katie, Summit99), no

significant correlation was found for the period 1934 to 1998. The central western correlation (based on cores D2, D3, D4, and D5) was found to be even higher than the Mosley-Thompson et al. (2005) results.

Chapter 3 Data and Methodology

3.1 Accumulation Data

In 2007, a field expedition named the NEEM Traverse and Survey was conducted by the Centre for Ice and Climate (CIC), University of Copenhagen and the Center for Remote Sensing of Ice Sheets (CReSIS) at the University of Kansas. As part of this survey, surface-based measurements of internal layer depth along a 375 kilometer segment of the Greenland ice divide connecting NGRIP and NEEM ice core sites (Fig. 3) were conducted using a 0.5 – 2.0 GHz FM-CW radar developed by CReSIS. Annual layers over the time frame 1889 to 2007 have been continuously tracked over the length of the traverse to obtain layer thickness. NEEM and NGRIP ice core records are available, and several shallow ice cores were collected along the traverse. These core data provide firn/ice density profiles and age-depth information that are used to maximize the accuracy of the radar derived annual accumulation. By using the thickness of the annual layers and ice core density profiles, annual water equivalent accumulation along the 2007 traverse path can be obtained more than one hundred years back in time.

Internal layering in the near-surface zone of the ice sheet is caused by seasonal variations in densification, sintering, and internal water vapor transport (Dibb and Fahnestock, 2004). A lack of melting in the dry snow zone and episodic snowfall events bury these layers over time, providing an annual record of accumulation. Density

differences of these annual layers result in local changes to the dielectric properties in the snow/ice media, which cause scattering of radar pulses that can be detected with a high frequency, high sensitivity FM-CW radar. This enables the radar to detect and track near-surface ice sheet internal layers (Rink, 2006). Hoar layers are the most visible layers in the near-surface firn, due to their density and crystal size contrast. This large contrast in density reflects electromagnetic energy substantially (Rink, 2006). Formation of hoar layers is caused by sublimation of ice crystals when heat flux is large. In central Greenland, strong summertime radiative heating of near-surface snow leads to strong temperature gradient and thus forms depth hoar (Alley et al., 1990). Boundaries of an annual layer are defined by adjacent hoar layers. Therefore, an ice year starts approximately in August and ends around the next August; annual accumulation is the amount of ice accumulated within an ice year.

Data collected by the radar are subsequently processed and visualized using CReSIS developed tools for Matlab environment. Matlab-based layer picker software developed by CReSIS is that main tool used to track the depth of annual layers (Fig. 4). The ice density profile along the traverse was assumed to be the same as the density profiles of the NEEM ice core. With layer thickness and an ice density profile, water equivalent annual accumulation rate can then be determined, counting layers back in time from the ice surface. The chronology of the layers is constrained by the age-depth profiles of the NEEM and NGRIP cores at each end of the traverse. The NEEM traverse, if separated into Southern and Northern sections by the point it bends to the northwest (at approximately at 76°N, 44°W), show different accumulation patterns. The southern section, located slightly more in the interior of Greenland, has a lower mean annual ice

accumulation (0.1543m/year w.e.) compared to the northern section (0.1721m/year w.e.). The most total ice accumulation of 1889 to 2007 occurred at the location of NEEM site. Moving southeasterly along the traverse from the NEEM site, the average annual ice accumulation amount decreases until the bend in the traverse, where the minimum accumulation is observed; south of this accumulation-minimum point, accumulation amount remains fairly constant to the NGRIP core site.

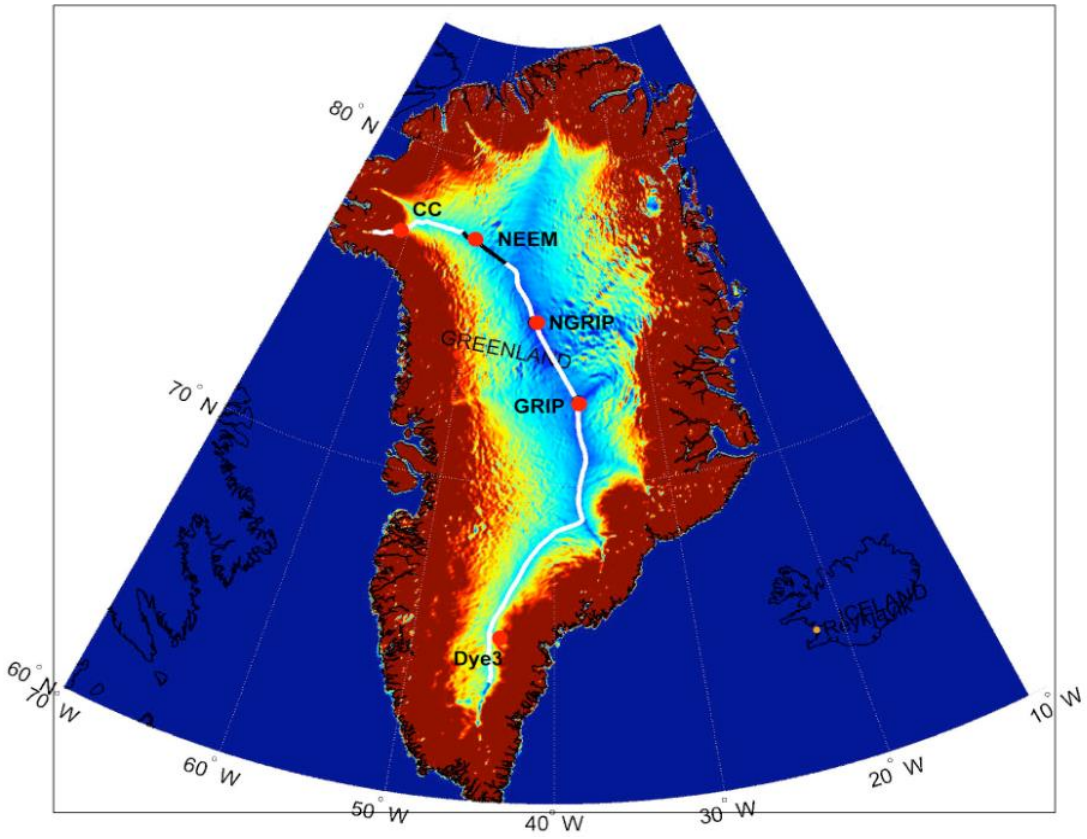

Fig 3. Location of the North Greenland Traverse, NGRIP and NEEM field camps in Greenland are shown; the white and blue line connecting the two sites shows the approximate route followed by both the surface traverse in 2007 and an airborne survey in 2011.

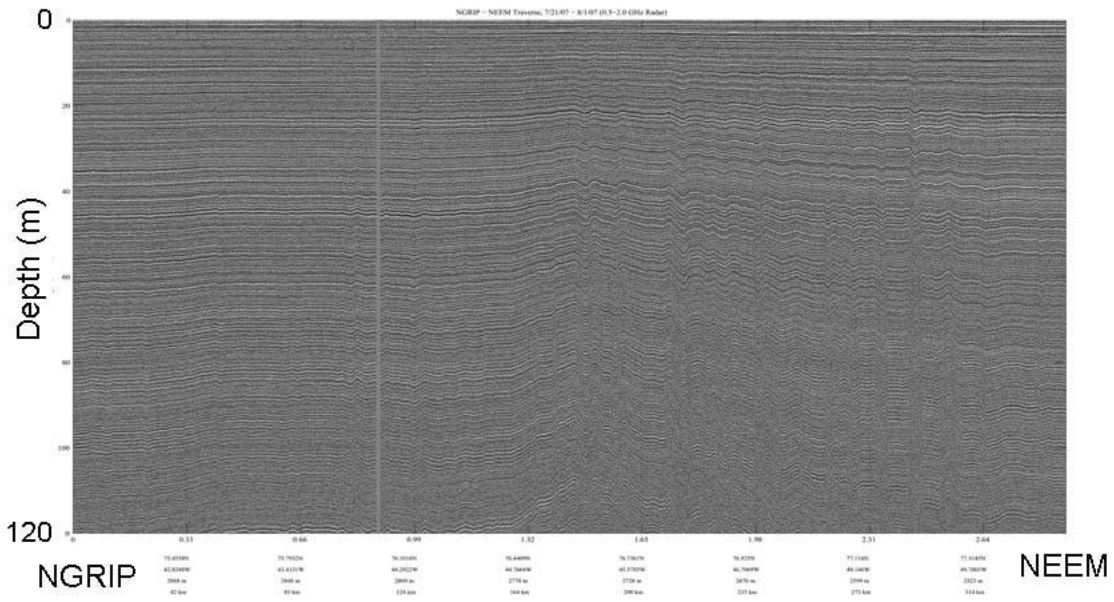

Fig. 4 Example of visualized ice sheet internal layers of NEEM traverse.

3.2 Meteorological Data

The NOAA-CIRES 20th Century Reanalysis Data - Version 2 (20CRv2) product (Physical Sciences Division and the University of Colorado CIRES Climate Diagnostics Center) is a 6-hour-resolved, 4-dimensional global coverage atmospheric data set that spans from September 1869 to December 2008 (Compo et al., 2011).The International Surface Pressure Databank (ISPD) version 2 (ISPDv2) is used for the production of 20CRv2. It is comprised of surface (land) and marine observations and tropical cyclone 'best track' pressure observations and reports. The station component is composed of various national and international SLP and surface pressure collections, with the International Surface Database contributing the largest proportion. International Comprehensive Ocean – Atmosphere Data Set (ICOADS) version 2.4 (for years 1952 – 2008 of 20CRv2) and version 2.5 (for years 1871–1951 of 20CRv2) (Woodruff et al.,

2010) are adopted for the marine component. An ensemble filter data assimilation method is applied to surface pressure reports; monthly sea-surface temperature observations and sea-ice distributions are used as boundary conditions. Compared to NCEP-NCAR Reanalysis data that starts in 1948, the 20CRv2 has an expanded time span to cover important climate events such as the 1920's warming period and the 1930's dust bowl droughts (Compo et al., 2011).

The 20CRv2 provides a large variety of variables. In this project, only precipitation rate and SLP are employed in the analysis. Precipitation rate is on a global Gaussian T-62 grid, given in the 20CRv2's yearly time series analysis fields; SLP is on a 2°x2° degree global lat/lon grid provided in 20CRv2's monthly synoptic fields.

The North Atlantic domain selected for this study is 0°W to 80°W, 36°N to 82°N, an area large enough that major storm tracks and cyclone systems potentially affecting Greenland's precipitation can all be included. The Azores Islands also lie within the domain, thus the full features of North Atlantic Oscillation can be displayed in the SLP maps. SLP data of the North Atlantic domain is interpolated into 100km x 100km Equal-Area Scalable Earth Grid (EASE-Grid). By doing this, all data points on a SLP map will represent grids of the same area, allowing equal weighting in the Self-Organizing Maps algorithm.

The NEEM Traverse and Survey accumulation data domain lies within a 1×6 sub-grid of the global Gaussian T-62 grid, covering 41.25°W to 52.50°W, 75.2°N to 77.1°N. Precipitation modeled by 20CRv2 shows that precipitation at the northern portion is constantly larger than southern portion by 30% to 40% during 1870 to 2008 period,

agreeing with the relatively higher ice accumulation observed by radar and ice cores. In this study, the average precipitation amount of the 1×6 Gaussian T-62 grid is used to represent overall precipitation of NEEM Traverse and Survey area. A 20CRv2 annual precipitation time series (Fig. 5) shows that a distinct offset took place in the early 1930s. For the time period of 1934 to 2008, 20CRv2 predicts mean annual precipitation in this area to be 34.82 cm/year, a value higher than previous estimates (Bromwich et al., 1998; Schunamann et al., 2009) by up to 10 cm/year; prior to this offset, the model predicts a precipitation rate of 52.28 cm/year, which is grossly overestimating the area's precipitation and is not supported by ice core and radar observations. This offset is believed to be cause by the limited availability of station and marine observations before the 1930s. Fig. 6 shows the total number of station and marine observations from ICOADS (Fig 6a) and ISPD (Fig. 6b) of 1870 - 2008, respectively. ICOADS statistic (Slutz et al., 1985) shows that the number of marine-based reports has experienced a rapid increase starting around 1940. There were peaks in the number of reports (mid 1910s, late 1920s, and late 1930s) prior to 1940; however, the numbers of reports since 1950 exceeded these peaks. For the North Atlantic region, report numbers only reached 10,000 per month before 1940 (mid 1910s, late 1920s, and late 1930s), while after the 1950s, more than 30,000 reports were available in almost all months; since 1960, the number of reports grew until it reached a maximum of more than 139,000. The International Surface Pressure Databank (ISPD) provides a comprehensive list of station (land) records, including coordinates and observation start and end time for each station. As shown in Fig. 6b, prior to 1940, very few surface pressure station reports were available in the North Atlantic region (less than 100, most of which are located in

Western Europe, including Iceland). Less than 5 station records were available annually in the Western Greenland and Baffin Bay domain before the 1930s, and less than 10 during the 1930s years. A rapid increase in the number of surface stations of both Western Greenland and Baffin Bay domain and the entire North Atlantic region occurred after 1940. Since 1960, in most years, there were reports from more than 1000 stations in the entire North Atlantic domain and more than 30 in the Western Greenland and Baffin Bay domain. Since the modeled precipitation is dependent on surface pressure, sea level pressure, and sea surface temperature (SST) reports, it is likely that the 20CRv2 model prediction's overestimation of precipitation in NEEM Traverse and Survey area prior to the 1930s is explained by the low number of reports. Due to the problem of unrealistic precipitation estimates, the year 1934 is chosen to be a point of transition based on the time when the distinct offset in modeled annual precipitation occurred. In this study, two separate analyses have been conducted: a more in-depth synoptic pattern analysis for the time frame 1934 to 2008, when more observations were available for surface analysis; and a similar analysis for 1870 to 2008 for comparison.

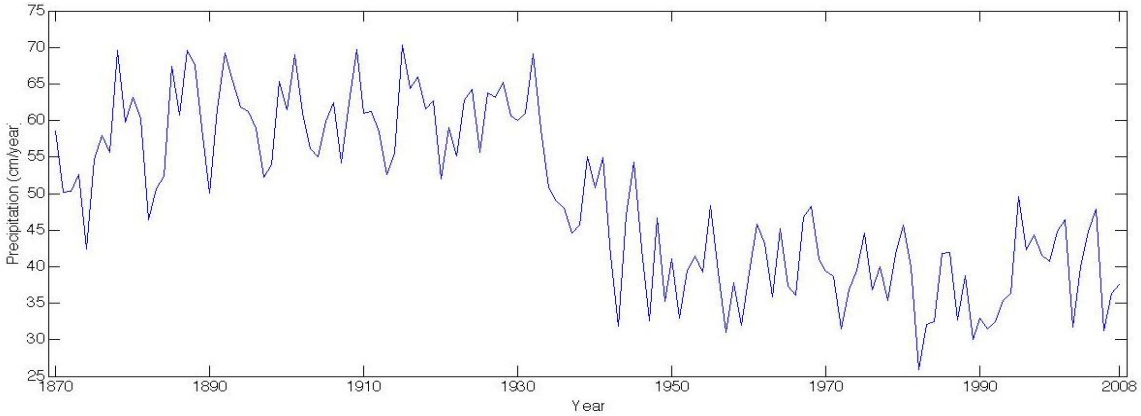

Fig. 5 Precipitation annual time series of the NEEM Traverse and Survey area based on 20th Century Reanalysis Data (Version 2)

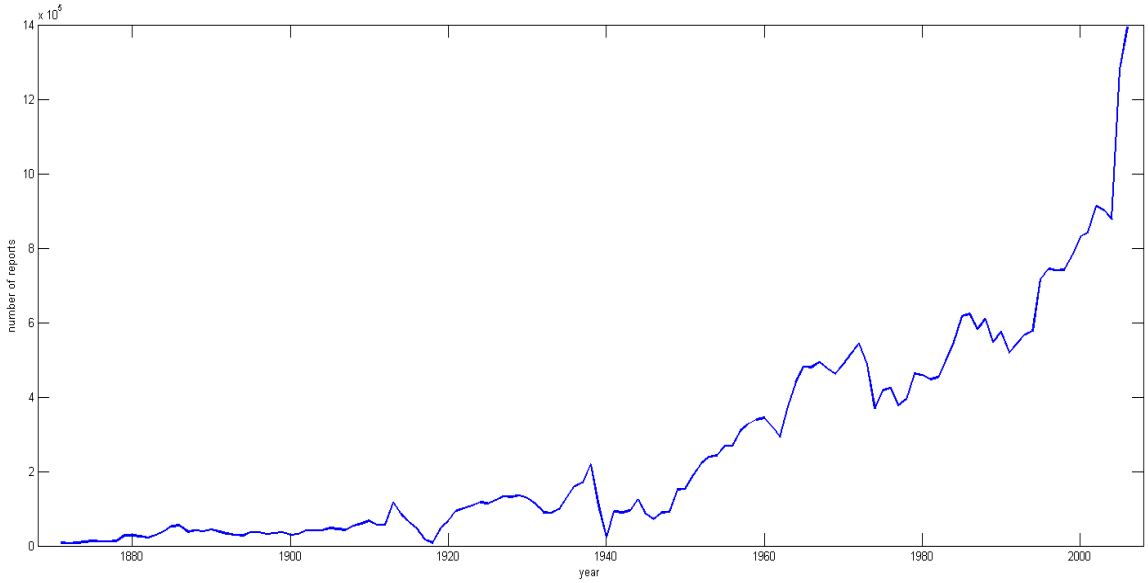

(a)

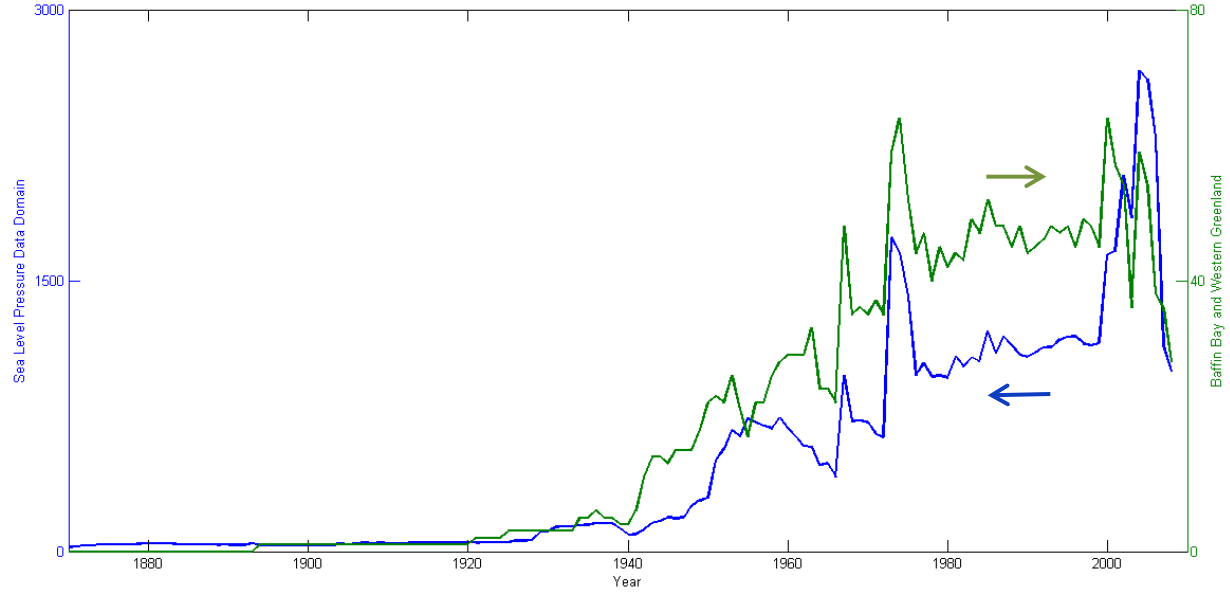

(b)

Fig. 6 (a) Number of yearly ICOADS North Atlantic region (SLP data domain, 0°W to 80°W, 36°N to 82°N) reports after duplicate elimination. (b) Number of surface pressure stations within 1) blue line: North Atlantic region (SLP data domain, 0°W to 80°W, 36°N to 82°N), left axis; 2) green line: NEEM Traverse and Survey and its neighboring area (80°W to 55°W, 70°N to 80°N), right axis.

For NAO index records, Hurrell Annual station-based North Atlantic Oscillation Index (NAOI) covering 1870 to present and a daily version of NAOI (based on the

Rotated Principal Component Analysis (RPCA) of monthly standardized 500mb height anomalies in the latitudinal range of 20°N-90°N) extending from 1950 to present is used. Appenzeller et al. (1998), Banta et al. (2007), Mosley-Thompson et al. (2005), Johannessen et al. (2005) all adopted this version of annual NAOI to study the correlation between NAO and precipitation and ice sheet changes in Greenland. NAM employed here are Hurrell wintertime SLP-based Northern Annular Mode (NAM) Index (annual) and daily NAM index (based on Empirical Orthogonal Function (EOF) analysis of monthly mean 1000-hPa (700-hPa) height anomalies pole-ward of 20°N latitude). Daily NAM covers the same time domain as daily NAO; annual NAM index extends farther back to 1899. These NAM data series were mostly used for studies on lower-latitude regions such as United States and Mexico. Few previous studies have related these data to North-central Greenland climatology.

3.3 The Self-Organizing Maps Algorithm

The spatial and temporal patterns of the North Atlantic domain's SLP maps from 1870 to 2008 have been obtained using the Self-Organizing Maps (SOM) algorithm, and these patterns have been compared with annual snow accumulation, daily precipitation record from 20CRv2, and daily and annual NAO and AO indices.

The SOM algorithm is a neural network algorithm used to analyze large amounts of high dimensional data and group them into a user-selected number of clusters (also referred to as units or nodes) through an unsupervised iterative training procedure. Every individual condition present in the original data set has a Best-Matching Unit (BMU,

defined as the node with least distance from the current condition) in the output nodes. All of the output maps together form an organized map, a two-dimensional array of patterns. The SOM algorithm was first introduced to a variety of disciplines by Kohonen et al. (1989, 1990, 1995). Hewitson and Crane (2002) applied it to climatology data to study synoptic scale circulation over north-east United States. Main et al. (1997) used SOMs to investigate seasonality of Southern Africa in general circulation models (GCMs). The SOM algorithm has also been applied for climate classification purposes in multiple studies (Malmgren et al., 1999; Cavazos et al., 1999, 2000). Previous work has shown the SOM algorithm's ability to understand large data sets of various structures and to categorize complex atmospheric circulation patterns into a manageable number of nodes. Furthermore, the SOM algorithm provides a means of visualizing these identified nodes as well as preserving the temporal continuity of the atmospheric circulations in the output maps.

In this study, the SOM algorithm is applied to 20CRv2 SLP data within the North Atlantic domain described above. This work was conducted using the SOM toolbox for Matlab (http://www.cis.hut.fi/projects/somtoolbox/). A user selected map size (SOM size) is required as input parameter for producing the optimal SOM. A map size too big results in the SOM having redundant patterns that are too similar to one another. A map size that is too small may lead to over-generalizing existing patterns (i.e. a single node representing multiple patterns might conceal significant atmospheric circulation patterns). In this study, map sizes ranging from 2×2 to 10×10 were tested. By applying elbow criterion (Tibshirani et al., 2001) to evaluate resulting quantification error (defined as average distance between each individual condition's present in the data set and its

BMU) and topographic error (defined as the proportion of all conditions present in the data set which its BMU and 2nd-BMU being non-adjacent node), the map size of 6×6 was found to be the optimal size. Visual inspection of similar map sizes (e.g. 5×7, 7×7, 8×8 etc.) was also done to ensure nodes in the 6×6 SOM extracted all significant SLP patterns; increasing map size beyond 6x6 only resulted in adding indistinguishable patterns and does not significantly reduce quantification error.

For the 6×6 SOM, the probability of any certain day's SLP pattern mapping to one of the 36 nodes is 1/36 or 2.78%. In other words, assuming every daily SLP pattern in the data set is represented by one of these 36 nodes (i.e. the BMU), then the expected frequency of occurrence for each node would be 2.78%. The following equation can be used to determine the significance of each node's frequency at 95% confidence interval (Schunemann et al., 2009):

$$p \pm 1.96\left(\frac{p(1-p)}{n}\right)^{1/2},$$

Here p is probability of any certain day's SLP pattern mapping to one of the nodes in the Master SOM; n is the number of daily SLP patterns used to produce the Master SOM (i.e number of days in the SLP data). In the 1934 to 2008 case, n equals to 27,363 (SLP data in 20CRv2 are missing dates: January 2nd, 1952- January 31st, 1952 and October 31st, 2000; n = 50,737 in 1870 to 2008 case, missing dates are: January 1st, 1870, January 2nd, 1952- January 31st, 1952 and October 31st, 2000. Therefore, if the frequency of a node falls outside the calculated interval of 2.58% to 2.97% (in the case of 1870 to 2008, 2.63% to 2.93%), it is considered either significantly high or significantly low.

Note that in Chapter 4, annual accumulation is compared with annual statistics of SOM node frequencies, although annual accumulation records are based on ice-year hoar layer development (a few months prior to the calendar year until a few months before the end of the calendar year) while annual statistics of SOM node frequencies are based on calendar year.

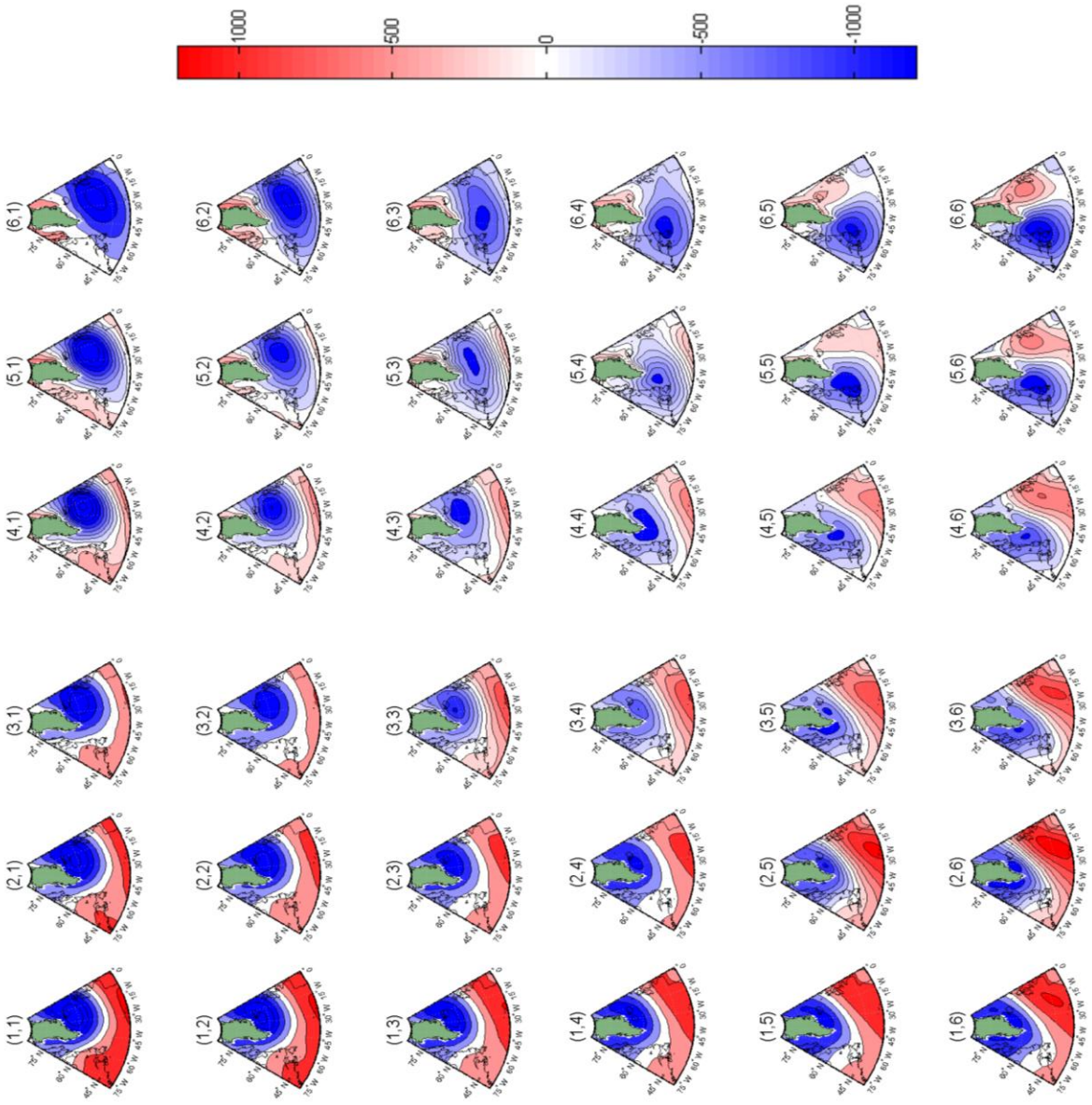

Fig. 7 Master SOM based on 20CRv2 SLP anomaly (Pa) from 1934 to 2008. Positive SLP anomalies are shaded in red, whereas negative SLP anomalies are shaded in blue.

Chapter 4 Results

4.1 The Master SOM

The SLP anomaly maps derived using the SOM algorithm is arranged in a 6×6 grid map, as shown in Fig. 7. This map will be referred to as the Master SOM. Each node is given a coordinate, e.g. (1, 1), (2, 1), based on their grid locations. As mentioned in the previous section, each daily SLP anomaly map has a BMU among the nodes in the Master SOM. Thus the Master SOM provides full coverage of all SLP anomaly cases that occurred in the 1934 to 2008 time frame. All meteorological features, including the North Atlantic storm track, Icelandic low, Azores High, etc., can all be found in the nodes. Within every node, negative SLP anomaly (blue) corresponds to low pressure, while positive SLP anomaly (red) corresponds to high pressure; their centers depict the centers of cyclones or anti-cyclones.

Focusing on the positions and intensities of low pressure systems in the Master SOM, the following general features are present: a northward shift of the low pressure system in every row from (6,X) to (1,X) (Here X is any column number); intensities of these low pressure systems tend to weaken in the middle columns, then re-intensifies and reaches another strong stage at the first column. Going from top nodes to bottom nodes in

any column (Example: from (X,1) to (X,6), X being any row number), low pressure systems shifts westward. However, intensity changes vary among different columns.

Several noteworthy cyclone tracks can be found in individual rows or columns. In the top row from right to left (from (6,1) to (1,1)), the Icelandic Low shifts northward towards Greenland's southeast coast, while increasing strength. In the first column (from (1,1) to (1,6)) from top to bottom, intensity of Icelandic Low weakens and shifts slightly towards the southwest, while the Azores High moves towards the Northwest of Azores Island. Along the bottom row from left to right (from (1,6) to (6,6)), the Icelandic low is near Iceland, shifts westward and weakens, and moves around Cape Farewell in southern Greenland. Then it intensifies and settles in eastern Canada. Meanwhile, the Azores High weakens and shifts northeastward until it is south of Iceland. In the last column from bottom to top (from (6,6) to (6,1)), the Azores High weakens. Low pressure located in the east of Canada moves eastward in the North Atlantic and becomes a vast system. Overall, from the left side to the right side of the Master SOM, the pressure gradient between the Icelandic Low and Azores High decreases; from top rows to bottom rows, changes in cyclone intensities are not monotonic, whereas changes in positions are also relatively small. Temporal evolutions of cyclone actions over time are shown in the Master SOM charactering all existing North Atlantic region SLP patterns and their evolution over time. An analysis of the nodes' daily transition over the time of interest provides some insights on the synoptic forcing leading to precipitation in North-central Greenland.

The SOMs generated using the full time length of 20CRv2 from 1870 to 2008 has no observable difference than Fig. 7, implying that prior to 1934, there is no significant addition of new, unique SLP patterns to those already shown in Fig. 7.

4.2 NAO and AO

The North Atlantic Oscillation (NAO) index is calculated using the difference of normalized sea level pressure (SLP) between the Icelandic low and the Azores high. When a strong Icelandic low as well as a strong Azores high is present, NAO index is positive. In positive NAO index scenarios, weather systems over the North Atlantic are more intense, while milder and wetter weather typically takes place in Western Europe.

Hurrell's annual and daily NAO Index and NAM (AO) Index are employed to verify the connection between these two indices and precipitation of North-Central Greenland, as well as their relations with node-represented SLP patterns. Daily NAO and AO indices are available from January 1st, 1950 through present; Annual NAO and AO indices cover 1864 through present. Only NAO and AO from days and years matching our 20CRv2 and NEEM Traverse Annual Accumulation availability are used. Mean and median as well as distributions properties of daily NAO and AO values for all days which SLP patterns mapped to each node in the Master SOM are calculated and analyzed (Figs. 8, 9), under the assumption that if any given daily SLP pattern is mapped to a certain node, it is considered to resemble the SLP pattern of that node. For all nodes, the corresponding daily NAO index follows a relatively peaked normal distribution (Fig. 8a; Kurtosis in the range of 2.48 – 3.70) with very small skewness (Fig. 8a; skewness between -0.49 – 0.18);

daily AO index distribution show similar features (Fig. 8b; Kurtosis and skewness in the range of 2.52 – 5.83 and -0.63 – 0.29, respectively.). Mean daily NAO index and daily AO index (Fig. 9a&b) are parameters serving the purpose of studying NAO and AO overall trend in the Master SOM; they are not actual NAO and AO values of their corresponding node's SLP patterns. Mean NAO and mean AO distributions are in general agreement: From the first column nodes to the sixth column nodes, mean NAO as well as AO indices decrease monotonically, as a southward shift of a low pressure system and northward shift of a high pressure system is present in the Master SOM. Nodes with highest mean NAO and AO are both shown to be Node (1,1); this node is characterized by the strongest Icelandic Low and strong Azores High. Moving downward along the first column (from Node (1,1) to Node (1,6)), mean NAO and AO decrease. One major difference in mean NAO and AO features shown by Fig. 8a and 8b is lowest NAO and AO nodes. Lowest mean AO is found in Node (6,1) , while lowest mean NAO occurred in Node(6,4) which is characterized by high pressure system close to Iceland and Azores Island surrounded by low pressure system. This difference is caused by latitudinal range of telecommunication patterns focused on by NAO and AO indices: NAO characterizes north-south dipole SLP anomalies, which one center is located over Greenland and the other between 35°N and 40°N in the North Atlantic; AO's calculation takes into account SLP anomalies of the Arctic region in higher latitude zones. Therefore when positive SLP anomalies are located farther north in the high latitudes and negative SLP anomalies are stronger in lower latitudes (Node (6,1)), mean AO is at its lowest.

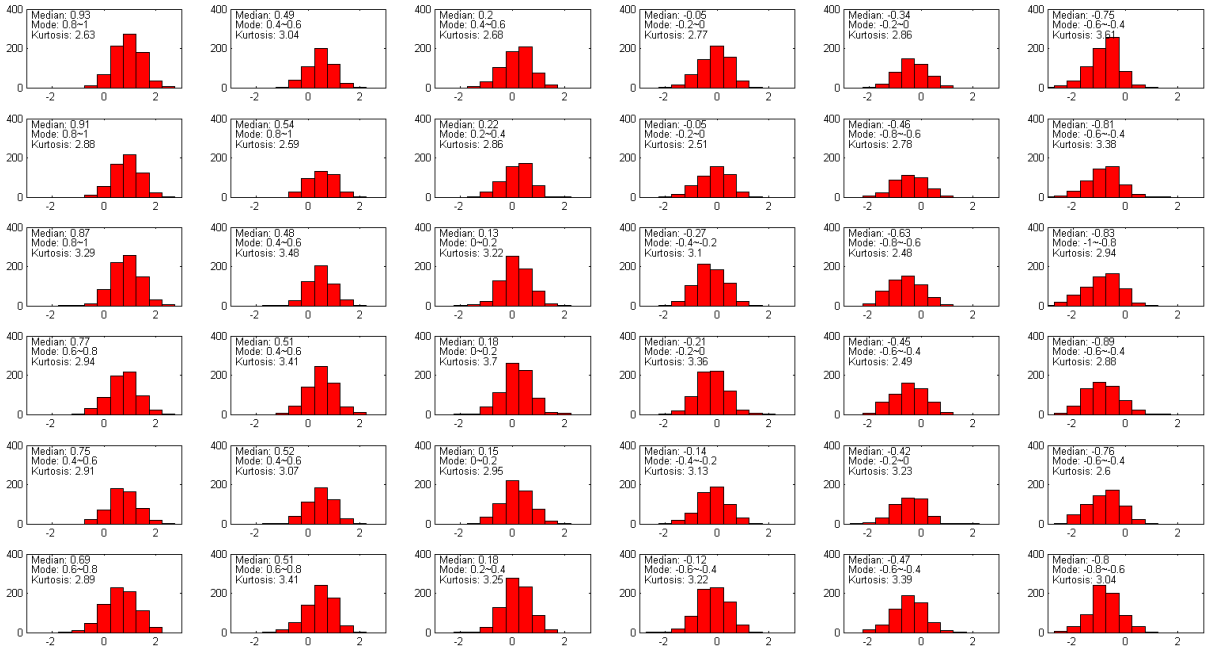

(a)

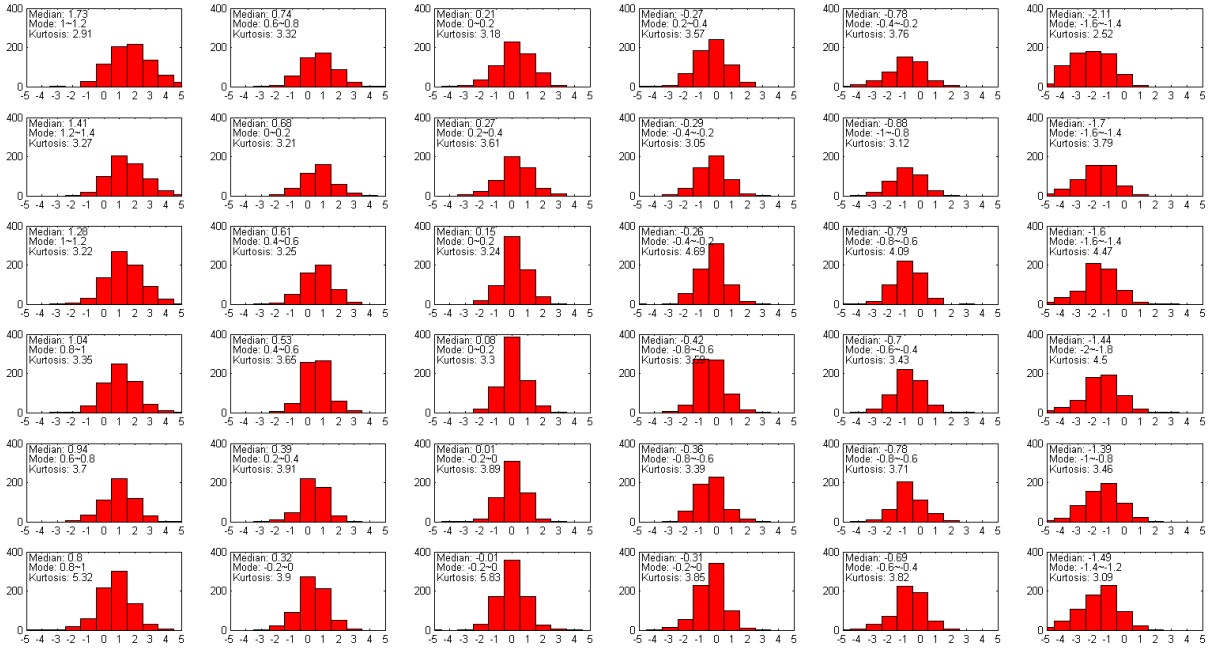

(b)

Fig. 8 Histograms of daily NAO (a) and AO (b) values for all days which SLP patterns mapped to each node in the Master SOM; each sub-plot corresponds to node of the same grid location in the Master SOM. Median, mode and kurtosis statistics are provided in sub-plots.

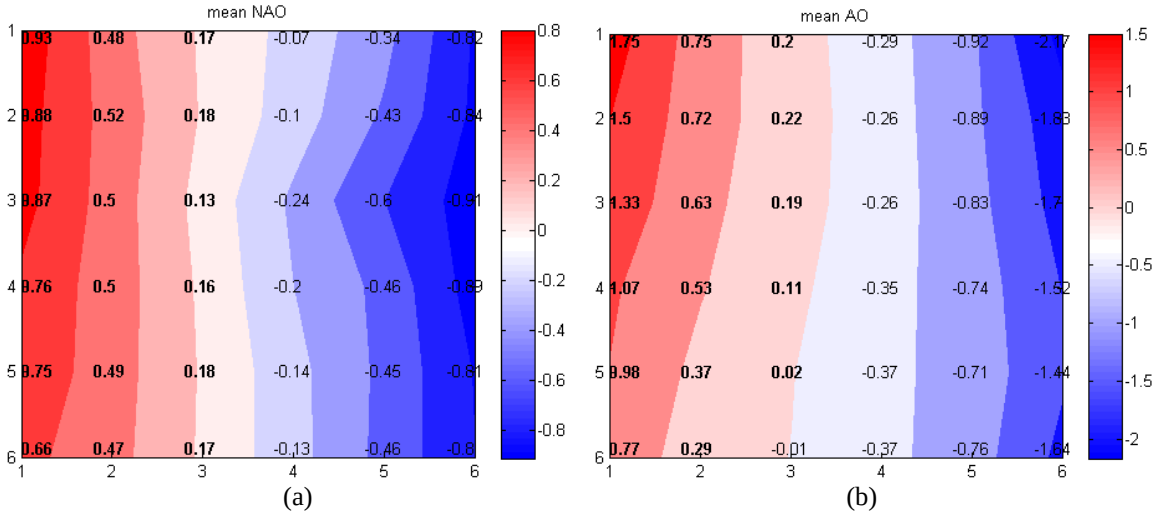

Fig. 9 Daily NAO (a) and AO (b) values for all days which SLP patterns mapped to each node in the Master SOM; positive values are bold and shaded in red; negative values are shaded in blue.

4.3 Daily Variations

Each node in the Master SOM has the chance to map to the current node, a neighboring node, or a non-adjacent node in the next day. Fig. 10 illustrates each daily node's evolutions. The three percentage values in the bottom of each node correspond to the percentage of SLP daily cases remaining in the current node, moving to an adjacent node (does not include diagonal nodes), and jumping to a non-adjacent node in the next day, respectively. The length of the arrow pointing a certain direction represents the chance of the current node moving to its adjacent node or diagonal node in that direction. These daily variation features eventually make up all synoptic transitions, including cyclone activities in the North Atlantic region and cyclone interactions with the GrIS.

One example of possible cyclone track is shown in nodes (3,6) and (4,6): a blocking of cyclone movement by the high elevations of the southern GrIS at the west coast of Greenland. These two nodes, showing similar features with a low pressure center just off the southwest coast of Greenland, both have a 30% chance of remaining in the same node

the next day. Furthermore, their long arrows pointing towards each other indicate high chances of moving back and forth between each other for a number of consecutive days, i.e. low pressure system stays off the southwest coast of Greenland. High precipitation nodes that persist for days will lead to a significant contribution in that year's total precipitation, thus impacting annual snow accumulation. Another possibly common pattern shown by the Master SOM and daily variation is splitting of cyclones in the Labrador Sea by the high elevation terrain of Greenland's southern tip. The beginning nodes of this cyclone track can be (4,4), (5,5), or (5,6); as we move left through Nodes (3,5), (2,5), (1,5), etc., a cyclone located near the southern tip of Greenland gradually splits into two smaller cyclones. The two new low pressure cyclones – one located west of Greenland in the Labrador Sea, the other near Iceland – are formed, as in Nodes (1,6) and (2,6). Note that the secondary cyclone, if it intensifies as it moves northwestward, can potentially develop into a polar low in colder seasons.

No evident distinctions are found between 1870 to 2008 and 1934 to 1870's node daily evolution patterns (Appendix: Fig. 20) besides the negligible difference in frequency statistics; all daily evolution features of 1870 to 2008 are also covered in the analysis described above. Therefore, a separate analysis of node daily evolution for 1870 to 2008 is not provided.

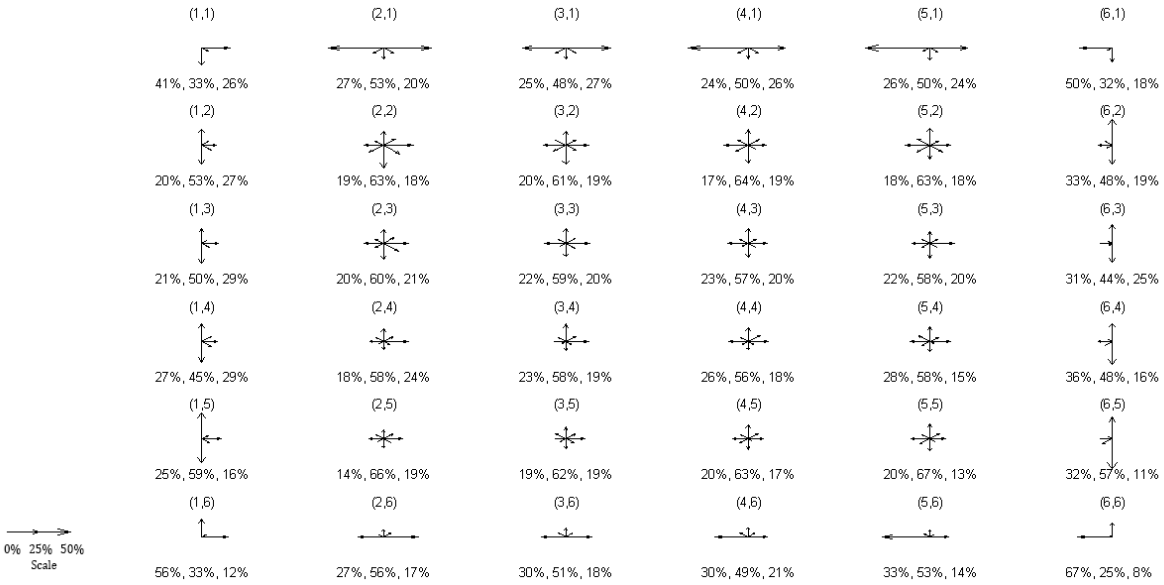

Fig. 10 Visualization of nodes' daily variations. Node coordinates are labeled at the top of each sub-plot. The three percentage values in the bottom of each node correspond to percentage of SLP daily cases: 1) remains in current node, 2) moves to an adjacent node (non-diagonal), 3) jumps to a non-adjacent node, in the next day. The length of arrow pointing a certain direction represents the chance (%, scale shown in lower left corner) of SLP daily cases of that node moving to its adjacent node or diagonal node in the arrow's direction.

4.4 Node frequency

As is discussed in the previous chapter, 2.58% to 2.97% is the expected range of frequency for a 6×6 SOM based on 27,363 daily cases (1934 to 2008), at 95% confidence interval. However, 28 out of 36 node frequencies fall outside this range (Fig. 11). Out of the 28 significantly different nodes, 15 nodes have significantly high frequencies. The bottom row (Nodes (1,6), (2,6), (3,6), (4,6), (6,6)), center nodes (Nodes (3,3), (4,3), (2,4), (3,4), and (4,4)), and nodes along the first column (Nodes (1,1), (1,3), and (1,4)) are three major clusters of these high frequency nodes. The bottom row nodes characterize cyclones located in the Labrador Sea moving north and being split by the southern tip of Greenland. In the previous section, we also found that when the cyclone position reaches

the southwest coast of Greenland, cyclone-blocking by GrIS's high elevation terrain may also occur. The center nodes (Nodes (3,3), (4,3), (2,4), (3,4), and (4,4)) depict cyclone moving around Cape Farewell, a pattern that is said to cause a large amount of precipitation in southern Greenland (Schunemann et al., 2009). Nodes in the first column (Nodes (1,1), (1,3), and (1,4)) share similar SLP patterns – a strong Icelandic Low and strong Azores High, which is a pattern associated with large positive NAO index. These three synoptic patterns comprised of multiple nodes occupy 43.24% of all daily cases, equivalent to 158 days out of every year; if associated with high daily precipitation in the North-central Greenland, these synoptic patterns can significantly contribute to annual snow accumulation.

Node frequencies of 1870 to 2008 are only slightly different from that of 1934 to 2008. The 1870 to 2008 frequency contour is almost identical to that for 1934 to 2008 (Appendix: Fig. 21). For the longer time series, 27 out of 36 nodes have frequencies that are considered significantly different at 95% confidence level (expected frequency range 2.63% to 2.93%). In both time frames, 12 out of 36 nodes are found to have frequencies larger than 3%.

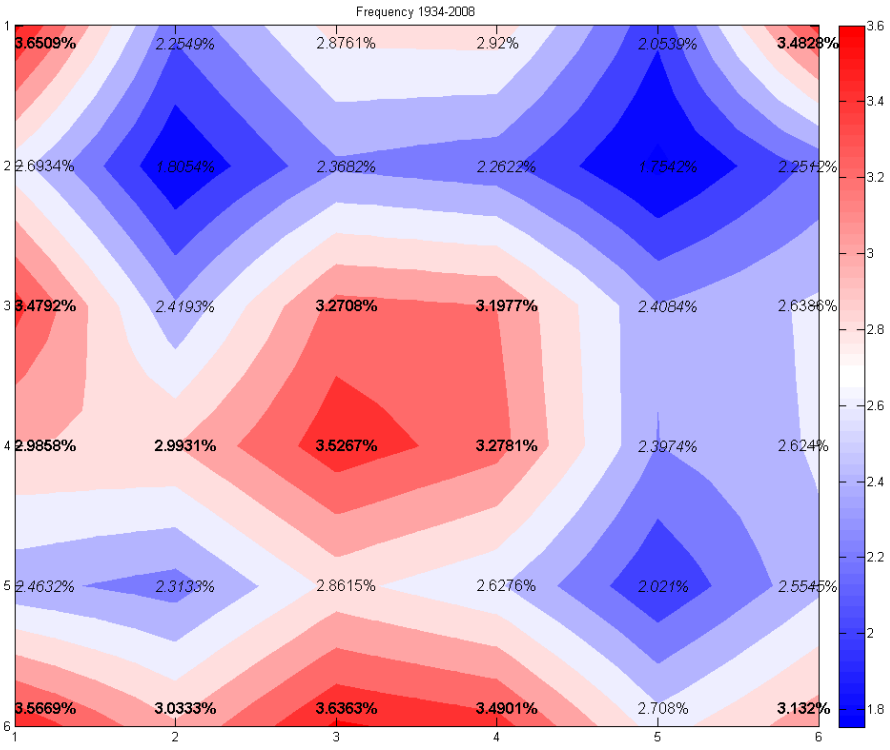

Fig. 11 Node frequency for 1934 to 2008 SLP SOM. Percentage numbers at coordinates show frequency of corresponding node in the Mater SOM. Percentage numbers of significantly high frequency nodes are bolded, while that of significantly low frequency nodes are italicized.

4.5 Precipitation

In the 20CRv2, precipitation is modeled based on surface pressure reports consisting of land and marine observations. SLP anomalies, a widely used means of representing atmospheric circulations at the surface, is a good reflection on complex synoptic and topographic forcing factors leading to precipitation in the North Atlantic region. In this section, 20CRv2 model derived precipitation of the NEEM Traverse and Survey area is employed for an in-model comparison with SLP anomaly SOM.

4.5.1 Daily Precipitation

Mean daily precipitation of all daily cases that map to a certain node within 1934 to 2008 is used to represent daily precipitation (mm/day) of that node. Fig. 12(a) shows average daily precipitation amounts for all nodes in the Master SOM. Nodes causing large daily (greater than 1mm/day) precipitation in the NEEM Traverse and Survey area are clustered in the lower proportion of the Master SOM under the quasi-diagonal connecting nodes (5,1) and (2,6) (Fig. 12(a)). Nodes in the Master SOM's lower-center (Nodes (4,5), (4,6), (2,5), (5,6), and (3,6)) has the highest daily precipitation values of greater than 1.30 mm/day.

For the 1870 to 2008 time frame, estimated node daily precipitation values are generally larger due to 20CRv2's greater overestimation of NEEM Traverse and Survey area precipitation prior to the 1930s. Nodes averaging large daily precipitations are similar to that of 1934 to 2008, focused in the lower central columns (columns 3, 4, 5) of the Master SOM (1.40-1.63mm/day), as well as the middle two nodes of the last column (1.55-1.66mm/day).

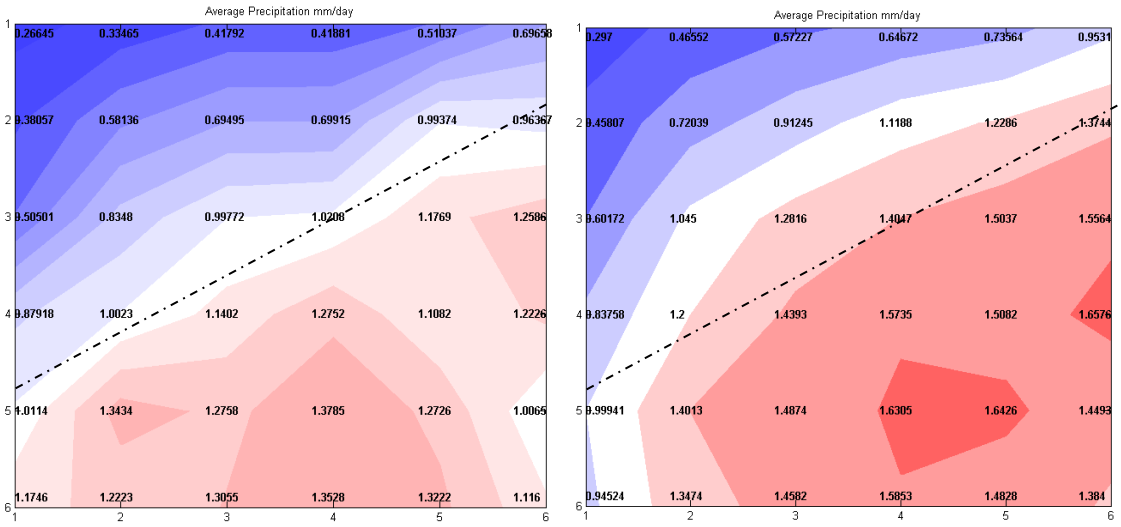

(a) (b)

Fig. 12 Average daily precipitation (mm/day) in NEEM Traverse and Survey area modeled by 20CRv2 for (a) 1934-2008, (b) 1870-2008. Numbers at coordinates shows 20CRv2 estimated average daily precipitation (mm/year) from corresponding node in the Master SOM.

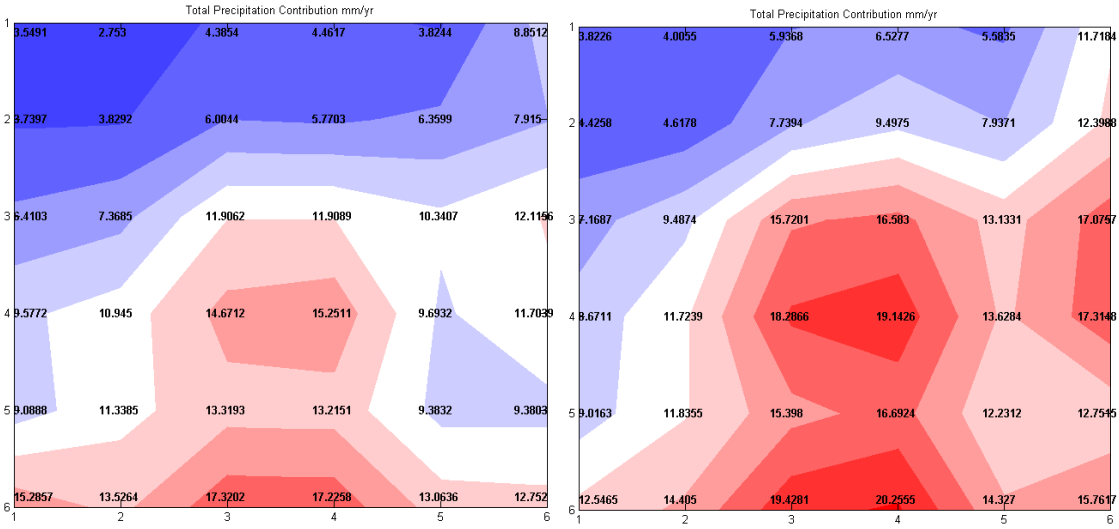

(a) (b)

Fig. 13 Annual precipitation contribution (mm/year) in NEEM Traverse and Survey area modeled by 20CRv2 for (a) 1934-2008, (b) 1870-2008. Numbers at coordinates shows 20CRv2 estimated annual precipitation contribution (mm/year) from corresponding node in the Master SOM.

4.5.2 Annual Precipitation Contributions

Annual precipitation contribution of a given node is determined by its amount of daily precipitation multiplied by the number of days it occurred during a year. As shown in Fig. 13(a), nodes with large precipitation (12.7-17.3 mm/year) contributions to the area of

interest's precipitation are mainly in the bottom two rows and lower half of central columns. Despite their highly daily precipitation, nodes in the lower half of columns 5 and 6 have slightly smaller annual contributions (9.3-12.1 mm/year) due to their lower frequency of occurrence.

The 20CRv2 estimates a total of 34.82 cm/year in the NEEM Traverse and Survey area for 1934 to 2008. The 11 nodes (30.6% of total nodes) in the bottom two rows and lower half of central columns ((3,3), (4,3), (3,4), (4,4), (2,5), (3,5), (4,5), (1,6), (2,6), (3,6), (4,6)) contributes 15.50 (154.9684) cm of annual precipitation, equivalent to 44.5% of total annual precipitation of this area. With nodes in the last two columns with slightly smaller annual contribution (i.e. (5,3), (6,3), (5,4), (6,4), (5,5), (6,5), (5,6), and (6,6)) included, a total of 19 nodes (52.8% of total nodes) are responsible for 70.0% of this area's total precipitation. Therefore, 20CRv2 data indicates that these nodes are major precipitation contributors for NEEM Traverse and Survey area.

The 19 major precipitation contributor nodes can be categorized into 3 groups based on the more general SLP patterns demonstrated. The first group consists of nodes (2,5), (1,6) and (2,6), which is characterized by strong Azores high and low pressure system located near east and west coast of Greenland. The second group include 8 nodes in the two middle columns (Nodes (3,3), (4,3), (3,4), (4,4), (3,5), (4,5), (3,6), (4,6)). These nodes are characterized by relatively weak cyclones in the Labrador Sea near the southern tip of Greenland; in Node (3,5), low-pressure center reaches its western-most location close to Baffin Bay. Azores High in Group 2 patterns are also weaker compared that of Group 1. In Group 3 nodes (Nodes (5,3), (6,3), (5,4), (6,4), (5,5), (6,5), (5,6),

(6,6),) low pressure system covers a large area of the Atlantic south of Greenland; a high pressure system lies either off the east coast of Greenland or farther south near Western Europe. SLP patterns shown by the three general groups of nodes are associated with positive NAO, neutral NAO around 0, and negative NAO, respectively. Two possible common storm tracks shown in these 19 nodes are: blocking of cyclones by the elevated GrIS and splitting of cyclones by the southern tip of Greenland. As already mentioned in section 4.2, cyclone blocking can be found in nodes (3,6), (4,6). Nodes (3,5) and (4,5) are also characterized by a low pressure system off the southwest coast of Greenland, and they will be regarded as nodes representing cyclone blocking as well. Splitting of cyclones is another common storm track found in the lower half of the Master SOM. An example of its possible process starts from Nodes (4,5), (5,5), (5,6) and ends in the left side nodes (1,6) and (2,6): an intense low pressure system southwest of Greenland in the Labrador Sea shifts north toward the southern tip of Greenland and weakens. After the splitting occurs at the southern tip, two new cyclones develop on both the southwest and southeast coast of Greenland. These two cyclones can potentially re-intensify; the cyclone on west side of Greenland can propagate farther north, possibly develops into a polar low in colder seasons, effecting Greenland's entire central-west Coast.

According to Fig. 11(a) and Fig. 12(a), when cyclones are located in the Labrador Sea (possibly secondary cyclones of cyclone-splitting at the southern tip of Greenland) southwest of Greenland (Group 1 and 2 patterns), the NEEM Traverse and Survey area receives the most annual total precipitation. When cyclones are farther south in the Labrador Sea near Canada (Group 3), NEEM Traverse and Survey area also receives high

daily precipitation. However, this occasion happens less frequently, possibly because cyclones shift away faster in the open ocean.

Nodes that have smaller average daily precipitation mostly result in smaller annual precipitation contributions to the NEEM Traverse and Survey area as well. There are two general types of SLP pattern in these nodes :1) Strongest Icelandic Low and a vast area of strong high pressure covering Eastern Canada, Azores Islands, and Western Europe (Nodes (1,1), (2,1), (3,1), (2,1), (2,2), (2,3), (1,3), (2,3), (1,4), (2,4), and (1,5)); and 2) Strong low pressure systems centered southeast of Greenland, covering Labrador Sea, Norwegian Sea and North Atlantic (Nodes (4,1), (5,1), (6,1), (4,2), (5,2), and (6,2)). In the first general pattern, the North-central Greenland region appears to be surrounded by low pressure. However, the 20CRv2 estimates limited precipitation under this situation, possibly implying that the high elevation terrain in Central Greenland (over 3000m) is blocking approaching cyclones. The latter SLP pattern demonstrates very few interactions between cyclones and Greenland topography, consequently there is limited precipitation predicted by 20CRv2 in the NEEM Traverse and Survey area.

The same analysis based on the full 20CRv2 extending from 1870 to 2008 produces similar results on the relationship of SLP patterns with precipitation in NEEM Traverse and Survey area. However, each node's daily precipitation and annual precipitation contributions extracted from 20CRv2 are significantly higher than the 1934 to 2008 case. This is associated with the distinct offset of modeled annual precipitation (Fig. 5) in the 1930s that was discussed in Chapter 3. Nodes with higher modeled daily precipitation are subject to higher levels of overestimate. Precipitation from SLP patterns showing strong

low pressure centered south of Greenland in the North Atlantic and Labrador Sea, as well as patterns in which a cyclone is moving around Greenland's southern tip are most overestimated. Group 2, Group 3, and Nodes (6,1), (6,2) shows the above SLP features; 20CRv2 estimates a total of 6.18 cm/year extra precipitation for 1870 to 2008 compared to 1934 to 2008.

4.6 North-Central Greenland Annual Snow Accumulation

The NEEM Traverse and Survey made radar measurements of annual internal layers along a 375km traverse along the Greenland ice divide, covering a large area over which elevation varied by a few hundred meters. Precipitation received in different parts of the traverse could likely be influenced by different synoptic forcing patterns. In this study, the NEEM Traverse is separated into a northern and a southern section based on the slightly different ice accumulation profiles mentioned in Chapter 3. Comparing the two sections, the northern section receives an average of 0.1721m/year w.e. accumulation, which is greater than the southern section which has a mean of 0.1543m/year w.e.. However, the standard deviation (σ) of annual accumulation for the southern portion (0.0353) is greater than that of the northern portion (0.0320), indicating relatively large annual accumulation variations. Very similar long-term patterns (Fig. 14) have taken place over the full range of the available years for northern and southern portions of NEEM traverse. An 11-year moving-average smoothing (Fig. 14) of northern and southern annual accumulation records shows a clear multi-year oscillation pattern. This pattern is present prior to the late 1980s, with a periodic cycle of approximately 20 years. The period with the largest amount of accumulation occurred in the 1940s for both bounds; the 1960s is also a high accumulation period. From the late-1980s to 2007,

annual accumulations in both bounds show increasing trends - trends only visible after smoothing and are otherwise overwhelmed by year-to-year variations. The individual year with the maximum annual accumulation for the Southern portion is 1944, with 0.2311m w.e. accumulation; the maximum annual accumulation year for the Northern portion is 1962, when 0.2454m w.e., accumulation occurred. However, no significant correlations are found between NAO/AO indices with both the northern and southern annual accumulation.

Annual accumulations of the ice sheet in the dry snow zone provide a means of assessing precipitation inputs to the ice sheet. As surface melting is very rare in this area, precipitation is mostly contained by the ice sheet and accumulates forming annual layers. High annual precipitation input in this area will result in more ice accumulation during that year; lower annual precipitation leads to a thinner annual layer. In this analysis, radar determined annual accumulation measurements from the NEEM Traverse and Survey are used as the single classification criterion to determine wet years, dry years, and average year between 1889 and 2007.

For both the Northern and Southern portions, 0.6σ and 1.2σ from each of their mean annual ice accumulation w.e. are chosen as thresholds to segregate wet years, dry years, average years, and extreme wet and dry years. Using these thresholds, wet and dry years are determined, with a sufficient number of extreme wet and dry years available, allowing a large enough sample size for investigating a connection between precipitation and synoptic scale patterns. If any year's accumulation (w.e.) falls within ±0.6σ from a 118-year mean annual accumulation (1889-2007), it is defined as an average year; when a certain year's accumulation is more than 0.6σ above the mean, it is defined as a wet year;

a year with accumulation less than 0.6σ below the mean is considered as dry year. Extreme years are defined as those which annual ice accumulation w.e. exceeds 1.2σ above (extreme wet year) or below (extreme dry year) the mean. Numbers of wet, dry, average, and extreme years extracted with this criterion are shown in Table 1. More wet years as well as dry years are present for the northern than the southern section.

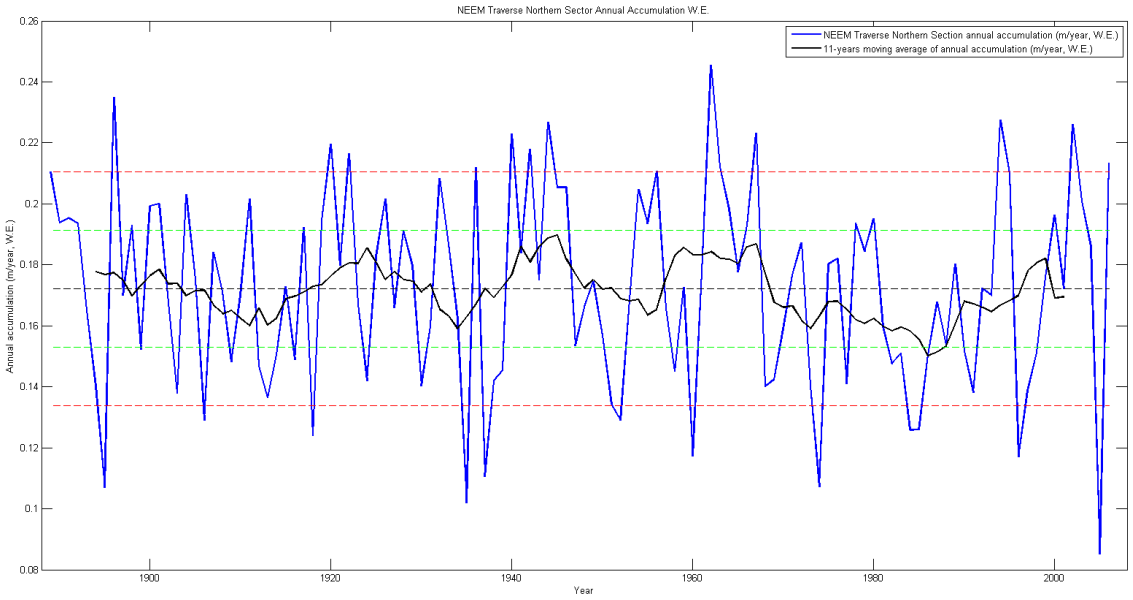

(a)

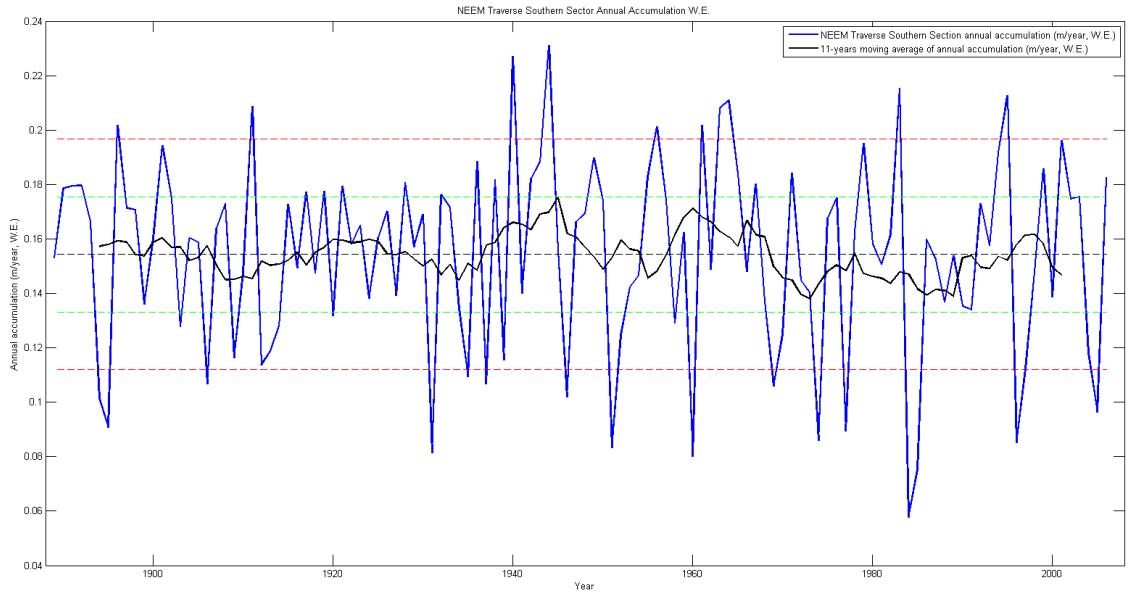

(b)

Fig. 14 Time-series of NEEM Traverse and Survey annual ice accumulation records for (a) Northern section of the traverse and (b) Southern section of the traverse. Blue lines show the annual ice accumulation (w.e.) over the period of 1889 to 2007; black lines are 11-year moving average of ice accumulation (w.e.) time series. The dashed lines in each figure shows 1.2σ above or below mean annual accumulation (w.e.) (red dashed line), 0.6σ above or below mean (green dashed line), mean annual accumulation (w.e.) (black dashed line). Years in which the annual accumulation (w.e.) amount is beyond the range of red dashed lines are extreme wet or dry years; years in which the annual accumulation (w.e.) amount is beyond the range of green dashed lines are wet or dry years; years in which annual accumulation (w.e.) amount falls between the two dashed green lines are average years.

Precipitation category / Section	Wet year	Dry year	Average year	Extreme wet year	Extreme dry year
Northern 1889-2007	38	37	43	15	12
Southern 1889-2007	34	28	56	10	16
Northern 1934-2007	22	24	27	11	12
Southern 1934-2007	23	18	32	8	12

Table 1. Number of wet, dry, average, and extreme years identified during 1889 to 2007 or 1934 to 2007, for the northern portion and southern portion of NEEM traverse

4.7 Synoptic Patterns in Wet, Dry, and Average years

In Section 4.3, major SLP patterns with the largest contributions to the NEEM Traverse and Survey area's annual precipitation identified based on 20CRv2 are 1) cyclone centered at the southern tip of Greenland, 2) strong cyclone in Labrador Sea or North Atlantic, 3) strong cyclone approaching the west coast of Greenland (in the order of higher annual precipitation to lower precipitation).

The NEEM Traverse and Survey annual accumulation data provides the most reliable measurement of annual precipitation for the interior of Greenland (dry snow zone) since the actual accumulation is preserved and the radar tracks continuous isochronous layers. Wet, dry, and average years are derived using this annual accumulation record and criterion described in the previous section. A wet year, i.e. a year of higher annual snow accumulation (w.e.), is the consequence of frequent precipitation events and/or a few very large precipitation events. On the other hand, little precipitation during the year will

result in a dry year. Analyzing prevailing SLP patterns of wet, dry, and average years using the Master SOM provides insights on the cyclone tracks and patterns responsible for the observed annual precipitation. Separate analyses are conducted for the NEEM Traverse Northern and Southern sections due to their different annual accumulation properties. A time period of 1934 to 2007 is chosen due to the higher number of data records available for these years, and also for a straight forward comparison with 20CRv2-based precipitation results as well.

The Master SOM of 1934 to 2008 is used to illustrate SLP pattern of the North Atlantic Region, assuming all these SLP patterns have the possibility to occur in wet, dry, and average years. Wet, dry, and average years' node frequencies are compared with a reference – overall average node frequencies for 1934 to 2007 along with its deviation from a reference value, as show in Fig. 15 to Fig. 18. Venn diagrams for distribution of significant nodes during wet, dry, and extreme years for both Northern and Southern sections are also given (Fig. 19). For a given type of year, high frequency node and nodes which their SLP pattern highly resembles high frequency nodes are chosen to fall into the circle for that type of year; pattern interpretation is applied in the production of the Venn diagrams.

Wet year node frequency changes for the Southern section (Fig. 15a) have the following general features: mostly-negative frequency change of right half of the Master SOM; positive frequency changes of nodes in the upper half of the 1st and 2nd column (Nodes (1,1), (2,2), (2,3), etc.) and lower-left corner nodes (Nodes (1, 5), (1,6), (2,6), etc.). The Master SOM shows that, Nodes (1,1), (2,2), and (2,3) experiencing positive

frequency change during wet years are characterized by strongest Icelandic Low and strong Azores High, corresponding to high NAO Indices. Additionally, the entire island of Greenland is surrounded by low-pressure system in these nodes. Lower-left corner nodes (1,5), (1,6), and (2,6) also have a strong Icelandic Low and Azores High, but shifted away from Iceland and Azores Island slightly; meanwhile another low pressure system centered at the west coast of Greenland is present – a possible result of cyclone-splitting occurring earlier at the southern tip of Greenland. These SLP patterns favoring wet years indicate that the existence of strong cyclones on either the west or east coast of Greenland is important in promoting precipitation in the NEEM Traverse Southern area. The cyclone flows associated with Strong-Icelandic Low patterns transports moist air from the ocean east of Greenland, creates onshore flow as it travels over the east coast of Greenland, and precipitates in the interior of Greenland. Similarly, nodes in the lower-left corner are associated with on shore flows conveying moisture from the ocean to the west. Other nodes experiencing slightly higher frequency during wet years are (5,4), (4,6), (6,1); these individual nodes are scattered in different parts of the Master SOM alone and may have limited impact on wet years' precipitation given they are single nodes. It is also shown that nodes with lower frequency during wet years are generally ones which have cyclones either farther away from Greenland's coast or of weaker intensity.

Dry year node frequency changes to reveal a pattern opposite to that of wet years. Frequencies of nodes with a strong Icelandic Low are lower, while nodes with weak Icelandic Low or high pressure over Iceland region became more frequent. Consequently, there will be a less flow that conveys moist air to the NEEM Traverse region through Greenland's east coast, resulting in less total precipitation in the year, thus less snow

accumulation in dry years. Higher frequency of nodes with cyclones centered close to Greenland's southern tip (Nodes (3,5), (4,5), (5,5), and (5,6)) is also observed. Frequent occurrence of these nodes in which a cyclone is at the southern tip of Greenland during dry years possibly implies that this type of cyclone track does not significantly contribute to precipitation in the NEEM traverse Southern area.

Nodes in the 1st and 2nd column (Nodes (2,3), (2,4), (1,6), (2,6), etc.) associated with strong Icelandic Low and Azores High also become more frequent in the Northern wet year patterns, similar to Southern patterns. Additionally, the upper-right corner nodes with a strong low pressure system farther south in the Atlantic Ocean with no clear interaction with Greenland, are also more frequent in northern wet years. Dry year node frequency change of the northern portion shows generally the same features as the southern dry year frequency changes. Higher frequency of nodes in the right half of the Master SOM (Nodes (4,3), (5,3), (5,5), (5,6), etc.) during dry years implies that, when weaker or more distant cyclones occur more frequently over the year, less total precipitation falls in the northern area of the NEEM traverse.

Average year node frequency changes for northern and southern portions of the traverse are mostly smaller in magnitude compared to that of wet and dry years, and within the range of -5% to 5%. Nodes with cyclones associated with larger amounts of precipitation in the NEEM traverse area occurs relatively often, but not as frequently as wet years; nodes with limited impact on precipitation do not occur too frequently, therefore in these average years, moderate amounts of precipitation are observed.

4.8 Extreme Wet Years and Dry Years

Extreme years are those which experienced exceptionally high (low) annual snow accumulation – 1.2σ above (below) the 118-year-mean annual ice accumulation (1889-2007). These years are rarer than the wet and dry years discussed in the previous section. The extreme years of southern and northern segments of the NEEM traverse for 1934-2008 will be inspected separately.

Node frequency changes based on the 8 identified extreme wet years of the southern portion (Fig. 17) shows highly distinguished features compared to that of regular wet years. Nodes which are more frequent during extreme wet years are mainly found in the lower-left section (Nodes (1,6), (2,5), (2,4), etc.) and right half of last row (Nodes (4,6), (5,6), (6,6), etc.) of the Master SOM. Though the upper-right corner nodes (Nodes (5,1), (6,1), (6,2)) and center right-side-columns (Nodes (5,4), (6,4), etc.) are occurring more frequently in extreme wet years than regular wet years, these nodes are also shown to be equally frequent or more frequent during extreme dry years as well as regular dry year. Moreover, the SLP patterns characterized in these nodes – high pressure system surrounding Greenland and low pressure system farther south in the Labrador Sea, do not show a strong connection with precipitation in the NEEM traverse southern area. Therefore, they are not considered to be significant contributors to precipitation during the extreme wet years. As is previously mentioned, lower left corner nodes characterize synoptic patterns with cyclones located off the southeast and southwest coast of Greenland; cyclones in these locations have the potential to convey moisture to the NEEM traverse southern area from either the Baffin Bay region or Greenland Sea in the east. Nodes on the right half of the last row (Nodes (4,6), (5,6), (6,6), etc.) are mostly

characterized by cyclones near the southern tip of Greenland; in these cases, when the low pressure system is deep and covers a large-enough area, it may still create strong onshore flow that can possibly lead to precipitation in the NEEM traverse southern area. High-frequency nodes for regular wet years in the upper 1st and 2nd columns of the Master SOM (Nodes (1,1), (2,2), and (2,3)) become almost neutral (i.e. very little deviation from their 118-year (1889-2007) average node frequency). This may indicate that synoptic patterns associated with these nodes are not the primary patterns leading to an extreme wet year. Infrequent nodes of extreme wet years are mostly characterized by a cyclone centered south of Iceland in the North Atlantic Ocean. These cyclones, no matter how strong or weak, are too distant from the NEEM traverse region to play a large role in precipitation over central Greenland.

Extreme dry year node frequency change patterns show the following features: Largest magnitude of frequency increase for nodes characterized by a strong cyclone in the North Atlantic south of Iceland (Nodes (5,1), (6,1), (6,2), etc.), high frequency increase for nodes with cyclones that are near the southern tip of Greenland (Nodes (3,5), (4,5), (5,5), etc.), and less frequent occurrence of nodes characterized by a low pressure system surrounding Greenland or centered near the west coast of Greenland. These features described above are in good agreement with regular dry year features discussed in the previous section; only the top right corner nodes (Nodes (5,1), (6,1), (6,2), etc.) are even more frequent in extreme dry years. It may be concluded that, when cyclones are more often farther south in the North Atlantic over the year, NEEM traverse southern area is more likely to experience a dry year.

It is found that regular wet and dry year node frequency change patterns for southern and northern portions of the NEEM traverse share much resemblance. However, a significant distinction in extreme wet year node frequency changes between the southern and northern portions was found (Fig. 17). Northern extreme wet years favor nodes characterized by a strong Icelandic Low and low pressure system surrounding Greenland (Node (1,1), (2,2), (2,3), (2,4), etc.), while southern portion extreme wet years favor nodes characterized by cyclones located both east and west coast of Greenland. Additionally, different from the southern portion, nodes in the right half of the Master SOM (For example, Nodes (6,1), (6,2), (5,4), (6,4), (4,6), (5,6) are a lot less frequent compared to southern portion extreme wet years) are mostly infrequent in northern extreme wet years. Extreme dry year node frequency change patterns of the northern segment is roughly the opposite of the extreme wet years: the high frequency of nodes characterized by a low pressure system in the south of Greenland (Nodes (5,2), (5,3), (4,5), (5,5), etc.) and nodes with a relatively weak Icelandic Low (Nodes (1,5), (2,5)). Similar features are seen in the southern portion extreme dry year patterns. The distinction in extreme wet year node frequency features indicates that the northern and southern domains have different synoptic forcing causing precipitation. Large amounts of precipitation in the northern area, which is closer to the west coast of Greenland, appears to depend more on a strong low pressure system dominating Greenland's entire region. The Southern portion is located further inland where the elevation is higher by several hundred meters. According to the results above, large amounts of precipitation fall in this area when cyclones are both west and east of Greenland, or when cyclones are centered very close to Cape Farewell, Greenland.

A separate analysis for 1889 to 2007 is conducted. Main features of wet, dry, and extreme year frequency change (Fig. 16 and 18) have shown to be consistent with 1934 to 2007's results described above, though percentage numbers may show small variance.

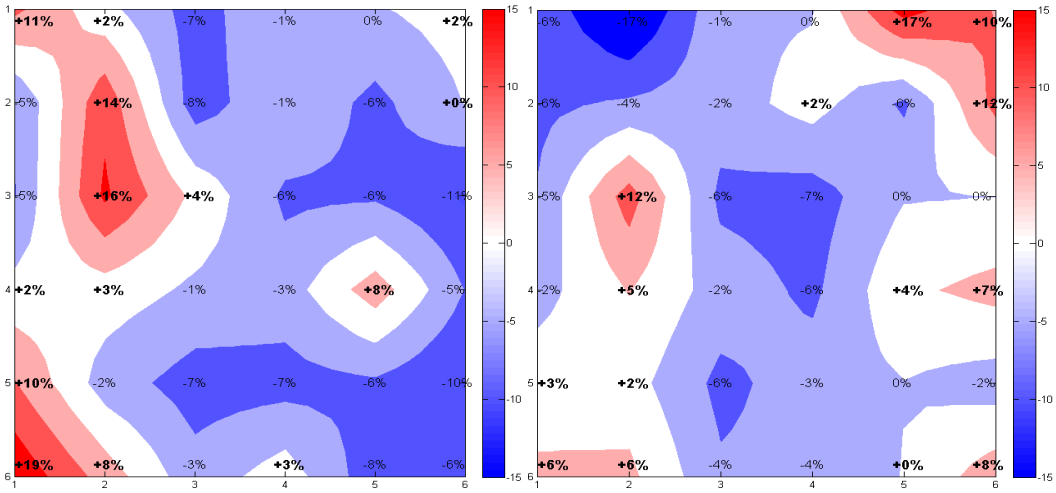

(a) Southern/wet

(b) Northern/wet

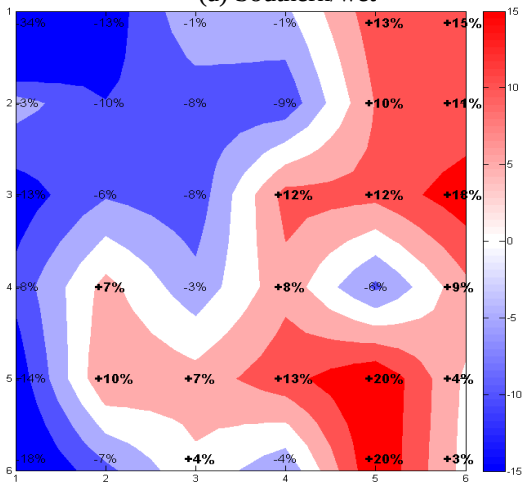

(c) Southern/dry

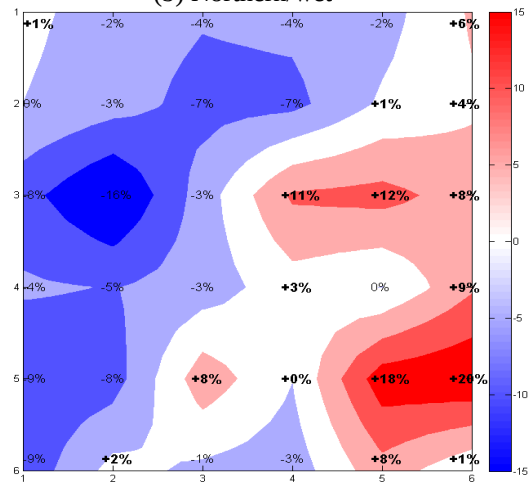

(d) Northern/dry

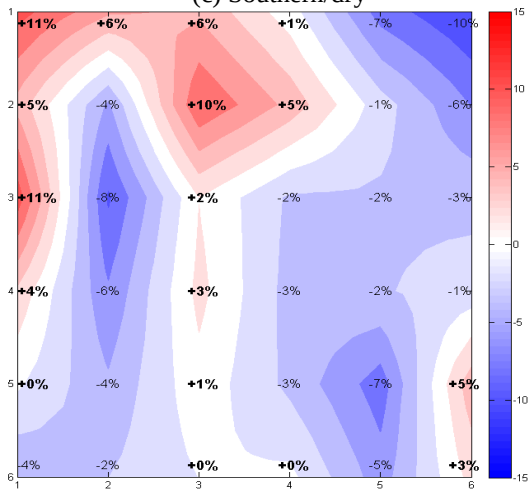

(e) Southern/average

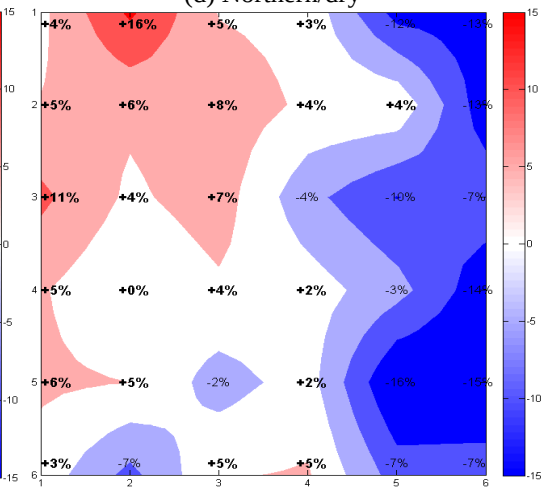

(f) Northern/average

Fig. 15 Node frequency change compared to 1934-2007 average, expressed in positive or negative percentage, for (a) Southern portion wet years, (b) Northern portion wet years, (c) Southern portion dry years, (d) Northern portion dry years, (e) Southern portion average years, (f) Northern portion average years. Positive percentage values are bolded and shaded in red; negative percentage values are shaded in blue.

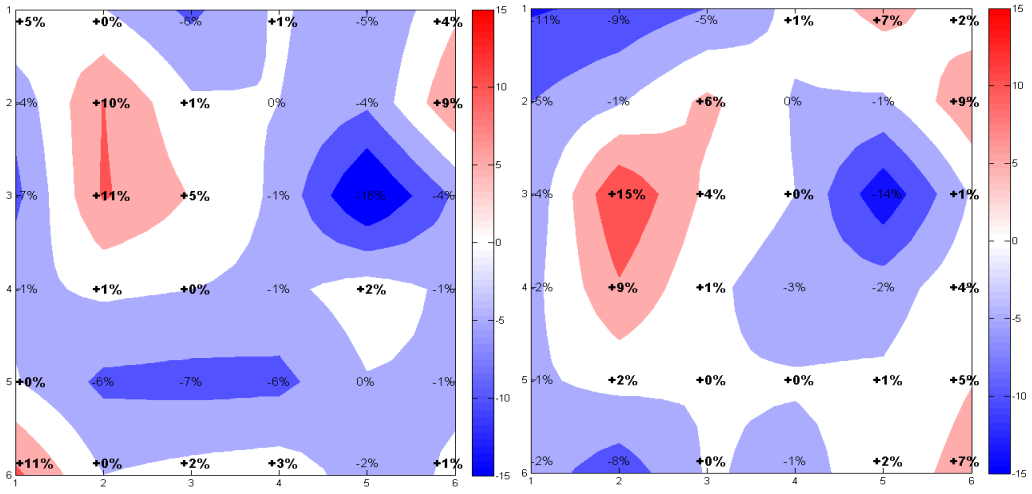

(a) Southern/wet

(b) Northern/wet

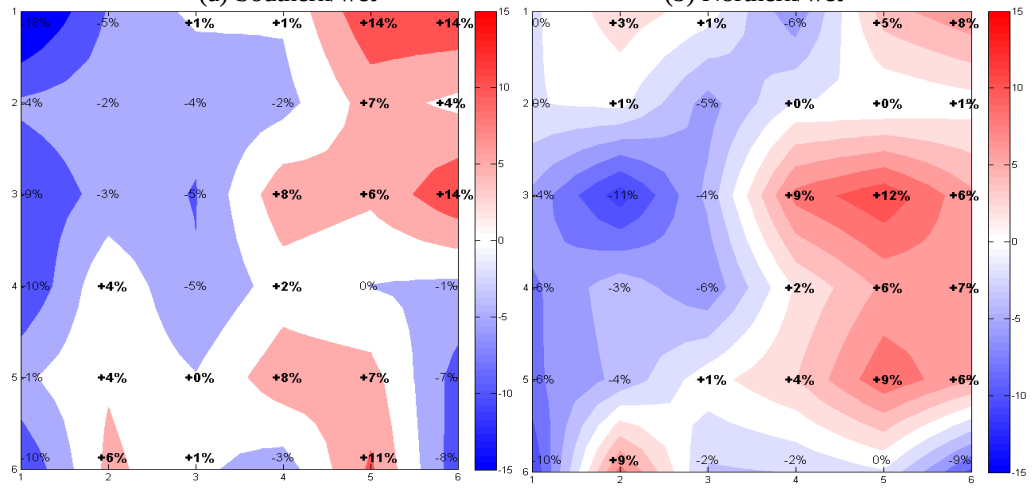

(c) Southern/dry

(d) Northern/dry

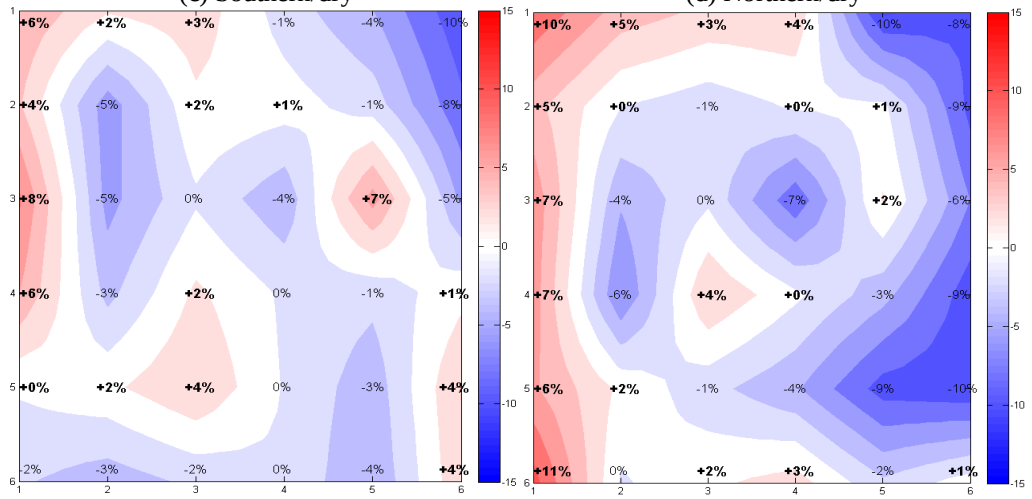

(e) Southern/average

(f) Northern/average

Fig. 16 Node frequency change compared to 1889-2007 average, expressed in positive or negative percentage, for (a) Southern portion wet years, (b) Northern portion wet years, (c) Southern portion dry years, (d) Northern portion dry years, (e) Southern portion average years, (f) Northern portion average years. Positive percentage values are bolded and shaded in red; negative percentage values are shaded in blue.

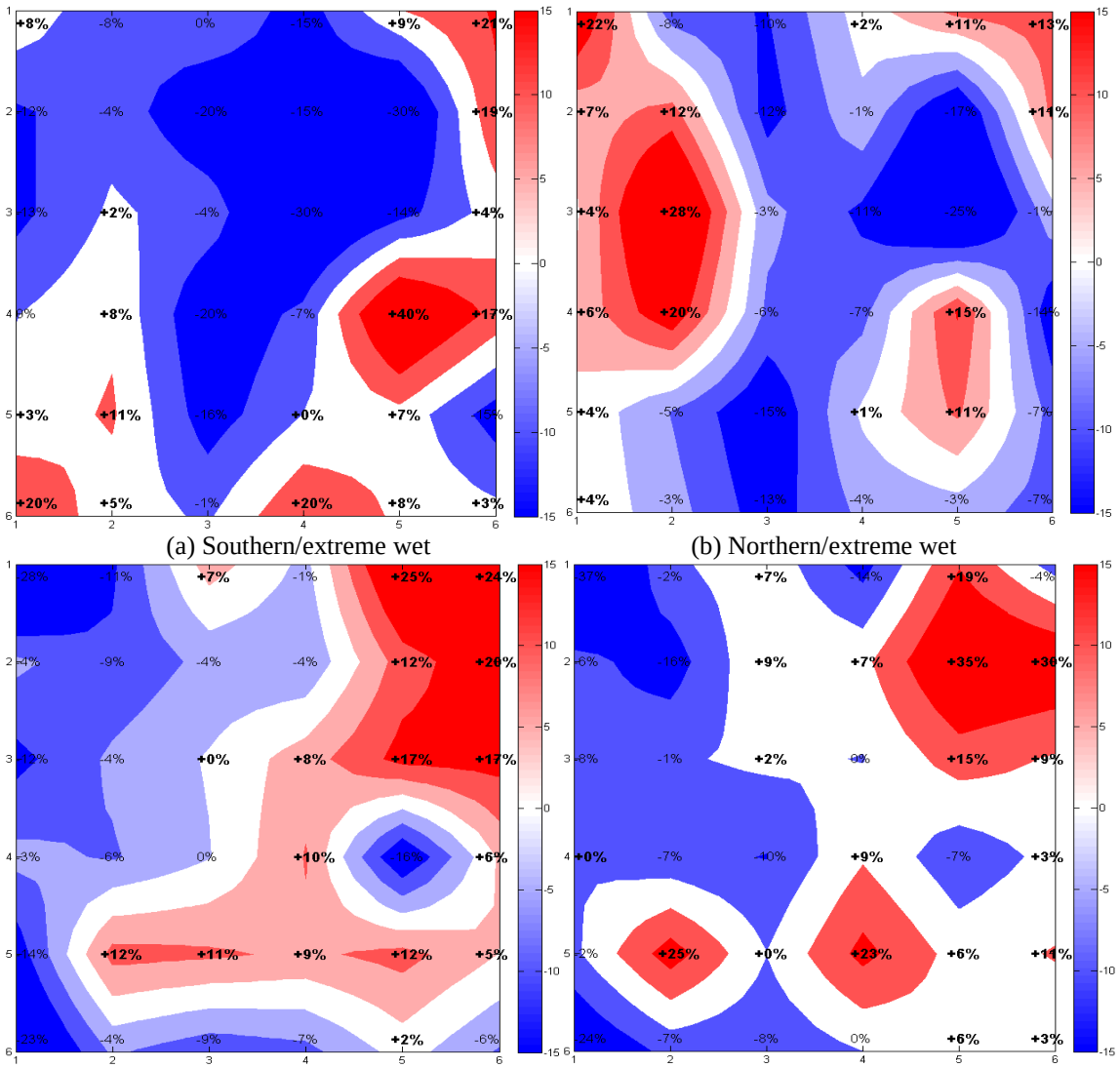

(a) Southern/extreme wet (b) Northern/extreme wet

(c) Southern/extreme dry (d) Northern/extreme dry

Fig. 17 Node frequency change compared to 1934-2007 average, expressed in positive or negative percentage, for (a) Southern portion extreme wet years, (b) Northern portion extreme wet years, (c) Southern portion extreme dry years, (d) Northern portion extreme dry years. Positive percentage values are bolded and shaded in red; negative percentage values are shaded in blue.

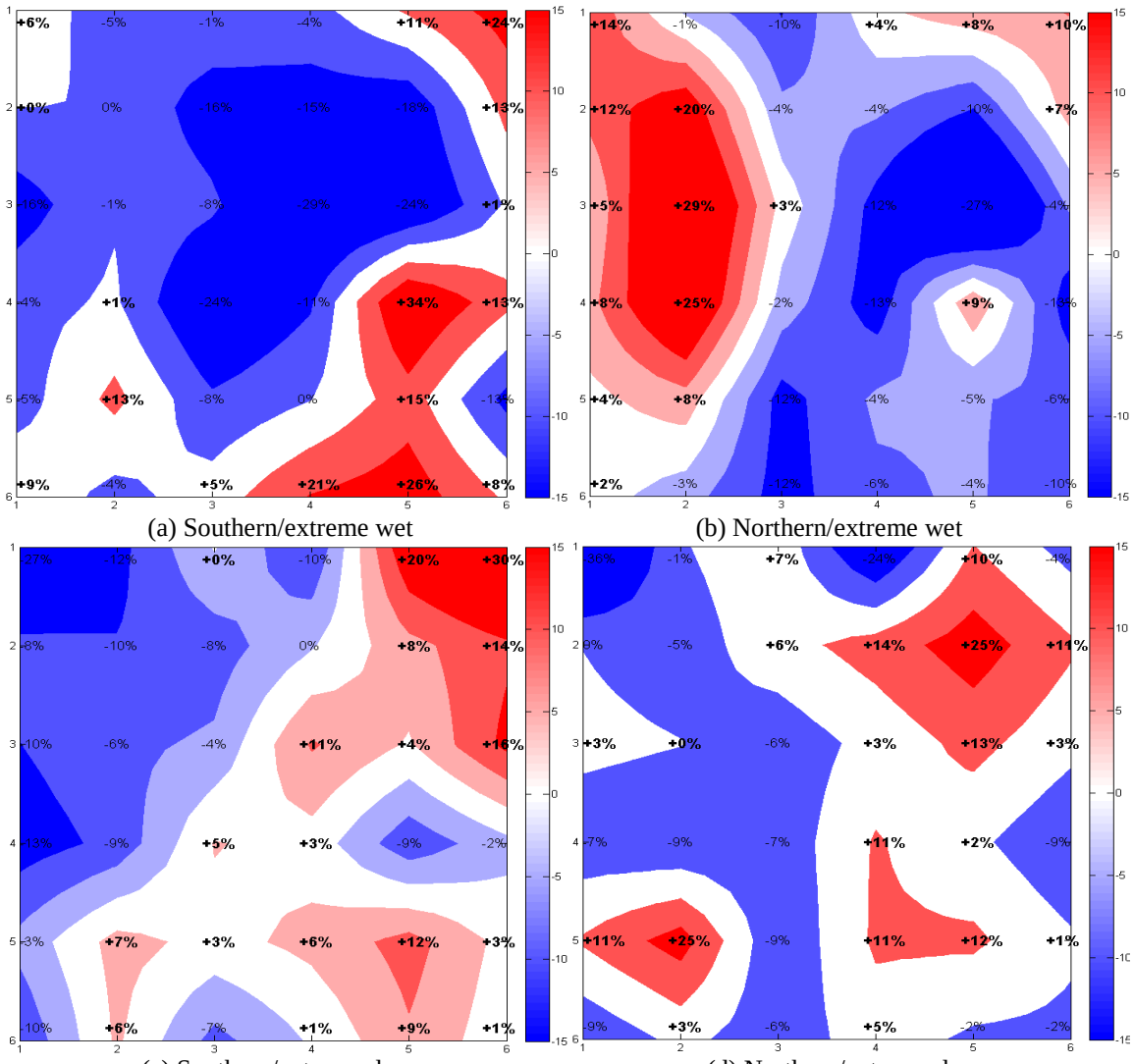

(a) Southern/extreme wet (b) Northern/extreme wet

(c) Southern/extreme dry (d) Northern/extreme dry

Fig. 18 Node frequency change compared to 1889-2007 average, expressed in positive or negative percentage, for (a) Southern portion extreme wet years, (b) Northern portion extreme wet years, (c) Southern portion extreme dry years, (d) Northern portion extreme dry years. Positive percentage values are bolded and shaded in red; negative percentage values are shaded in blue.

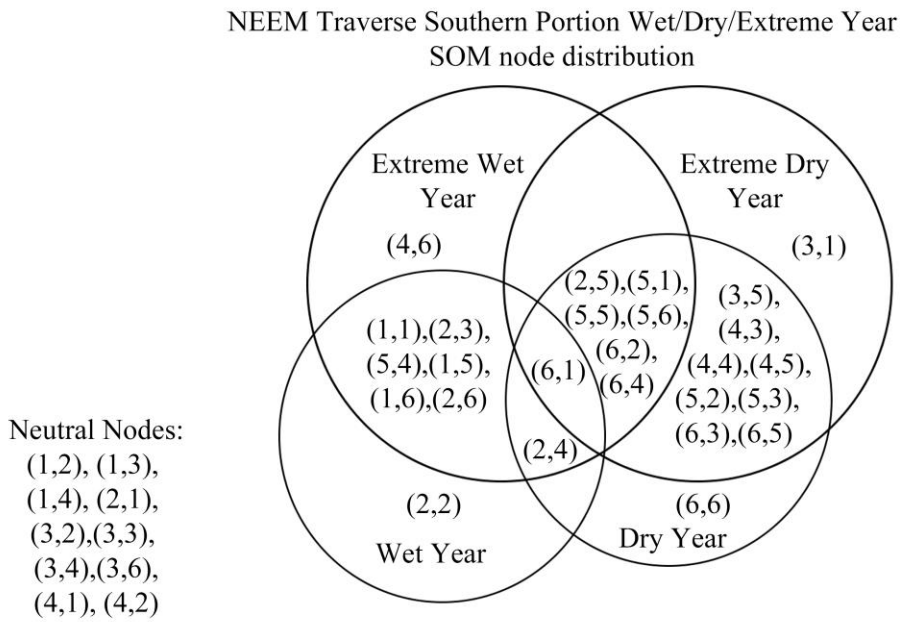

(a)

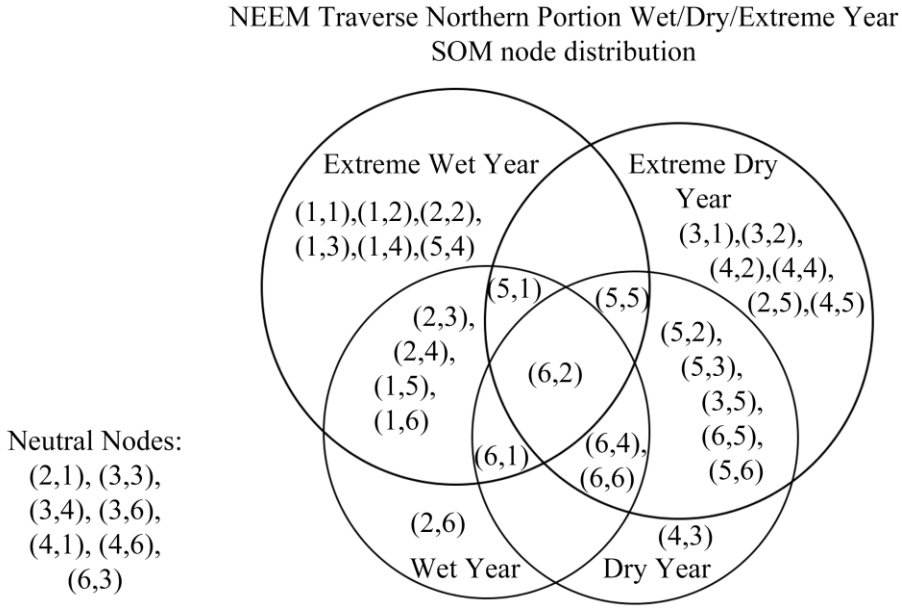

(b)

Fig. 19 Venn diagram for SOM nodes segregated based on their frequency of occurrence during wet, dry, and extreme years of (a) Southern portion and (b) Northern portion.

Chapter 5 Discussion and Conclusions

5.1 Discussion

The purpose of this study is to find synoptic scale forcing factors contributing to precipitation of North-Central Greenland. The main data sets employed to serve this purpose are the 20CRv2 SLP fields and modeled precipitation and NEEM traverse and Survey radar-derived annual snow accumulation records. The analysis has emphasized the post-1934 data for its superior station/marine observation coverage over pre-1934 years; analysis for the full data set is also conducted (1870-2008 for in-model synoptic pattern analysis and 1889-2007 for model-radar-based synoptic pattern analysis). The NEEM Traverse and Survey radar-measured annual snow accumulation records is major advance over previous studies base on climate models, reanalysis data, and ice core records (Ohmura and Reeh, 1991; Ohmura et al., 1996, 1999; Thompson and Pollard, 1997; Glover,1999; Murphy et al., 2002; Dethloff et al., 2002; Box et al., 2004, 2005, 2006; Hanna et al., 2005, 2006, 2008; Fettweis et al., 2008; Ettema et al., 2009). The NEEM traverse annual snow accumulation records from CReSIS provide better spatial representativeness, fewer uncertainties, and more than one century of observed dry snow zone precipitation; in addition, the 375 km-long traverse allows this data to reliably represent a much broader area than ice cores.

The Self-Organizing Maps methodology provided a means of classifying and visualizing SLP patterns and their day to day change that are present in the 20CRv2 daily SLP data, which allows for a comprehensive cyclone track/synoptic forcing factor analysis. Compared to Schunemann et al. (2009) which is based on 39-year ERA-40 data, this study has a longer time-span of SLP data and precipitation/annual accumulation records. Over one hundred years of daily SLP cases, modeled daily precipitation, and annual snow accumulation enables extraction of adequate numbers of wet year/dry year for a solid statistical analysis as well as a long-term comparison with NAO/NAM records. Daily-resolved SLP data is able to capture slight changes in cyclone movement and intensity, which will otherwise be masked in data products under lower temporal resolution.

The Master SOM derived 36 nodes representing all SLP pattern daily featured in 20CRv2 SLP data (1934-2008). Despite small differences in data domain selection, SLP patterns displayed in these 36 nodes include nearly all features in Schunemann et al.'s (2009) 5×7 SOM. The Master SOM, combined with node frequency and day-to-day evolution features, enables the following potential cyclone tracks within the North Atlantic region to be identified: cyclone-blocking at the west coast of Greenland due to high elevation of southern GrIS, cyclone splitting by Greenland's southern tip, and other cyclones' intensification/weaken accompanied by shifts in location. Cyclone splitting and blocking are also found by Schunemann et al. (2009) using ERA-40 SLP fields. Similar interactions between cyclones and the high-elevation portion of southern Greenland has also been referred to in research based on case studies and climate models (Chen et al. 1997; Kristjansson and McInnes 1999; Petersen et al. 2003; Tsukernik et al. 2007).

However, cyclones originating in Baffin Bay and approaching Greenland from the west, which is a common cyclone track according to several previous studies (Schunemann et al., 2009; Chen et al., 1997), is not clearly shown in the Master SOM: this may be caused by difference between 20CRv2 and ERA-40. An overall trend of NAO and AO indices associated with each node's SLP pattern in also present in the Master SOM: NAO and AO indices of nodes decreases monotonically from the left side of Master SOM to the right side.

In-model analysis (20CRv2 based SLP SOM versus 20CRv2 precipitation) and model-versus-radar analysis (20CRv2 based SLP SOM versus radar-measured annual snow accumulation) lead to distinctly different results on determining the main synoptic forcing factors on North-central Greenland precipitation input. 20CRv2 daily precipitation data for North-central Greenland estimates 34.82cm/year of annual precipitation, which is an overestimation of more than 15cm/year for some portions of the traverse (Ohmura and Reeh 1991; Chen et al. 1997; Ohmura et al. 1999; Bales et al. 2001; Cassano et al. 2001; Box et al**.,** 2004, 2005, 2006). Nodes identified as providing the largest contribution to both daily and annual precipitation are characterized by cyclones centered near the southern tip of Greenland (possibly in the process of splitting) or farther south in the Labrador Sea. These SLP patterns possibly contribute to enhanced precipitation by advecting moist air to Greenland. Chen et al. (1997) mentioned that, when a cyclone travels around Greenland's southern tip (or Cape Farewell), a great amount of precipitation usually falls in southern Greenland. However, no clear evidence or previous research indicates that these patterns may lead to notable precipitation events in North-central Greenland (NEEM traverse area). According to Schunemann et al

(2009)'s study based on ERA-40, similar SLP patterns are regarded as major precipitation contributors in southern Greenland; in regions farther north, these patterns were associated with very little daily/annual precipitation.

The NEEM traverse annual snow accumulation records provide a unique assessment of annual precipitation for central Greenland. The NEEM traverse has been separated into two segments – the northern and the southern segments due to slight differences in their annual snow accumulation climatology. The northern segment is located closer to the west coast of Greenland and has a lower overall elevation; the southern segment is farther in the interior of Greenland, and its average elevation is higher than the northern segment by several hundred meters. These regional differences may lead to different precipitation forcing factors: the northern segment may be more susceptible to cyclones approaching from the west of Greenland, while it can be more difficult for these cyclones to affect the southern segment. Over the 118 years (1889-2007) of available accumulation records, using w.e. annual snow accumulation as gauge for annual precipitation, wet/dry years and extreme wet/dry years can be well defined on a regional scale and can be segregated from average precipitation years (see section 4.4 for detailed criterion for distinguishing wet/dry years, average years, and extreme years). Though several previous studies have reported a negative correlation between NAO index and western Greenland annual accumulation based on ice core records (GITS, NASA-U and D2) over various time intervals (Appenzeller et al., 1998; Mosley-Thompson et al., 2005), the NEEM traverse annual snow accumulation records show no significant correlation with either NAO or AO index.

Analysis of SLP pattern frequencies for wet/dry years in the southern portion show that prevailing SLP patterns in wet years are those characterized by high positive NAO index, i.e. a strong cyclone located near Iceland (or shifted slightly towards Greenland's southeast coast). SLP patterns in which a cyclone is located 1) south of Greenland in the North Atlantic ocean, or 2) in the Labrador Sea south of Cape Farewell, occurs less frequently during wet years; these same SLP patterns have also been shown to be more frequent in southern sector dry years. A common feature shared by these patterns prevailing in dry years is very little interaction between cyclones and Greenland topography. It can be inferred that cyclones need to be close enough to GrIS so that interactions between the cyclone and Greenland topography are possible, and thereby creating onshore flows that transports moist from maritime areas to the North-central region.

Surprisingly, in extreme wet years and extreme dry years of the southern sector, a notable number of SLP patterns that occur at higher frequencies are overlapping. These overlapping patterns are mostly associated with low NAO indices (negative or neutral). It is worth mentioning that extreme wet and extreme dry years mostly occur during the 1930s to 1980s period, when NAO undergoes a long period of neutral/negative values. Extreme wet and dry years that are clustered during low-NAO periods may imply a connection between annual NAO index and the magnitude of year-to-year precipitation variability over a longer time frame. However, southern sector regular wet years' high frequency SLP pattern do not occur more frequently in extreme wet years.

SLP pattern frequency features for northern sector wet years and dry years are very

similar to that of the southern sector: more frequent occurrence of 1) high-NAO-characterized SLP pattern and 2) SLP patterns with cyclones at the west coast of Greenland during wet years; high frequency of SLP patterns characterized by cyclones centered south of Iceland/Greenland, in the North Atlantic ocean during dry years. This similarity between northern and southern wet and dry years indicates that synoptic forcing factors for these two areas may be similar to a quite large extent. Unlike the southern extreme years' distribution, northern extreme wet years and dry years are more evenly distributed throughout the entire time domain, covering periods of high and low NAO. Therefore, SLP pattern frequency for these years does not favor either positive-NAO or negative-NAO. Instead, regular wet year SLP pattern frequency properties become stronger during extreme wet years; likewise, extreme dry years have also displayed strengthened dry-year SLP pattern frequency features.

Despite that regular wet and dry year climatology of the northern and southern sectors have a lot in common, this difference in extreme year SLP pattern found between the two sectors in this study implies that a difference in synoptic forcing exists, and could be caused by several reasons. One possible reason is a connection between the southern sector precipitation variability and the long term trend associated with NAO, while precipitation in the Northern sector is impacted more by cyclones approaching from the west of Greenland. Difference in geo-location of the two bounds may also play a role: the southern sector is located farther away from Greenland's west coast and several hundred meters higher in altitude as well; chances are that topography and distance from the coast may play a bigger part in the more-elevated southern area. Despite all the possible explanations, it is worth-mentioning that attempting to explain precipitation patterns of

the region of interest solely depending on SLP-base synoptic patterns may not be adequate, since North-central Greenland has extremely high elevation. More in-depth and comprehensive analysis can be done in the future if more parameters are taken into account, e.g. temperature, humidity, and seasonal precipitation patterns.

Schunemann et al. (2009) studied precipitation forcing factors of central and western Greenland (the NEEM traverse lies within these Schnemann et al. defined regions). For both these regions, Schunemann et al. also found that when a broad area of low pressure is surrounding Greenland or a cyclone is located off the west coast of Greenland, higher amounts of precipitation fall, which is in agreement with results in this study. Wet year/dry year prevailing SLP patterns in this study also provide insights into connections between the NEEM traverse area precipitation with NAO, which previous studies found no significant correlation (Appenzeller et al., 1998; Bromwich et al., 1999; E. Mosley-Thompson et al., 2005; Hurrell et al., 2003, 2009).

Analysis for 1889 to 2007 does not significantly change the main features of wet, dry, and extreme year frequency change, though the percentage of cases may show a small variance. It is likely that this small change in individual node frequency is related to long-term climatic patterns in the North Atlantic region.

The climatology of North Atlantic region over the past 118 years addressed in this study provides insights into synoptic forcing of precipitation/snow accumulation variability of North-central Greenland. These findings can help predict future North-central Greenland precipitation trends by examining changes in synoptic scale patterns simulated by General Circulation Models (GCMs).

5.2 Conclusions

The Self-Organizing Maps (SOM) algorithm is applied to 20CRv2 SLP fields; 36 SLP patterns are chosen to represent all synoptic features in the North Atlantic region. These SLP patterns in the Master SOM are used to evaluate 20CRv2 modeled-precipitation of North-central Greenland as well as to seek synoptic scale patterns leading to wet/dry years in North-central Greenland based on radar-measured annual snow accumulation. Key findings are:

1) No long-term trend in w.e. annual accumulation change is observed during 1889 to 2007 for both Northern and Southern sectors of the NEEM traverse. Before the 1980s, there is an approximately 20-year periodic cycle of annual accumulation. An increasing trend of annual accumulation occurred from late 1980s to 2007.

2) Movements, changes in intensity of cyclones and anti-cyclones are displayed. Possible main cyclone tracks interacting with Greenland's topography are: 1) cyclone splitting at the southern tip of Greenland, and 2) cyclone-blocking by the high-elevation ice sheet in western Greenland. Other cyclone tracks and strengthening and weakening patterns are also found.

3) SLP patterns characterized by a vast low pressure system surrounding Greenland or cyclones approaching Greenland from the west are identified as prevailing wet year patterns for both southern and northern sectors. Dry years favor SLP patterns characterized by cyclones centered far away from Greenland, mostly in the Labrador Sea or North Atlantic. Precipitation usually results from cyclones that convey moisture from neighboring oceans and creates on-shore flow. This

requires sufficient interactions between cyclones and Greenland topography. If during a certain year, a large number of days are characterized by very little interaction between cyclones and Greenland topography, then this is likely to be a dry year.

4) Extreme wet/dry years SLP pattern properties showed that distinctions in climatology exist between the northern and southern sectors of the NEEM traverse. This distinction is possibly due to SLP patterns identified in 20CRv2 having different degrees of impact on these areas' precipitation; there may be topographic factors or distance to the coast influencing precipitation of the farther inland, higher-elevated southern sector.

This study has also shown that caution should be taken when using 20CRv2 model estimated precipitation of North-central Greenland. Annual precipitation derived from radar measured snow accumulation records is only possible at annual resolution. However, the 20CRv2 does not properly estimate North-central Greenland's precipitation, and also appears to mask certain SLP patterns (cyclones originated in Baffin Bay) that were found in other studies. Seasonality of precipitation as well as important precipitation events are also masked in annual snow accumulation records. Applying the SOM algorithm to a SLP field of reanalysis data, polar lows cannot be distinguished from midlatitude cyclones, and thus their contributions in precipitation. Using higher temporal resolution precipitation records as well as higher temporal resolution cyclone data may provide more comprehensive and in-depth explanations to the climatology addressed in this study. Studies have

found that decades of high correlations between NAO and Greenland surface air temperature (SAT) alternates with decades of low NAO-SAT correlations (Hurrell, 1995; Polyakova et al., 2006). This indicates a connection between circulation patterns and SAT at decadal scale; therefore, North-central Greenland precipitation amounts may also be sensitive to SAT. However, this study did not look into is connection. In the future, SAT can be included as a parameter to assist segregate wet and dry year and identify wet year, dry year, and extreme year synoptic patterns. By doing this, explanations to some complicated results of this study (e.g. some wet year and dry year synoptic patterns overlapping, especially in NEEM traverse southern portion extreme years) may be better addressed.

In summary, future improvements of this study could incorporate more meteorological parameters (e.g. SAT), seasonality properties, and incorporating Regional Climate Models to examine the meteorological forcing mechanisms of precipitation/accumulation in North-central Greenland.

Appendix

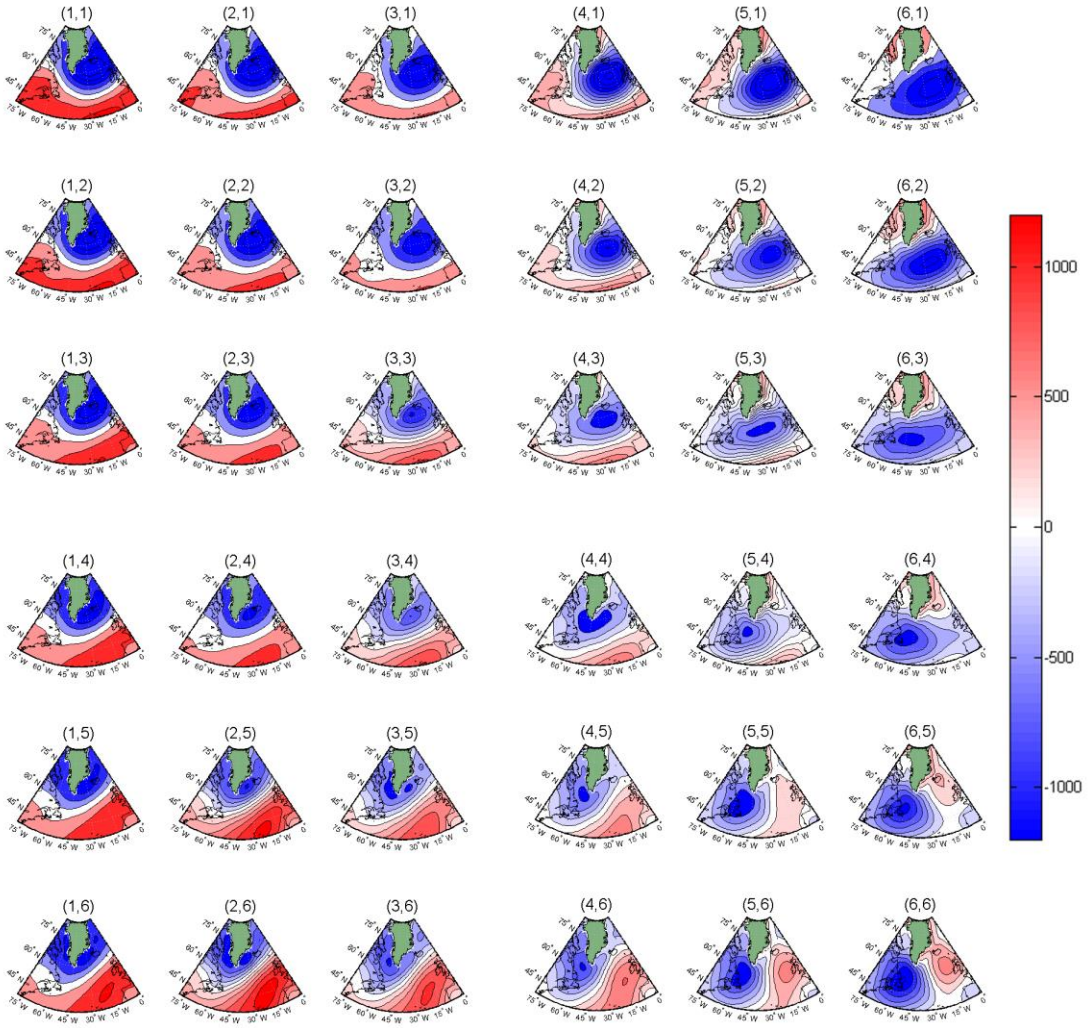

Fig. 20 Master SOM based on 20CRv2 SLP anomaly (Pa) from 1870 to 2008. Positive SLP anomalies are shaded in red, whereas negative SLP anomalies are shaded in blue.

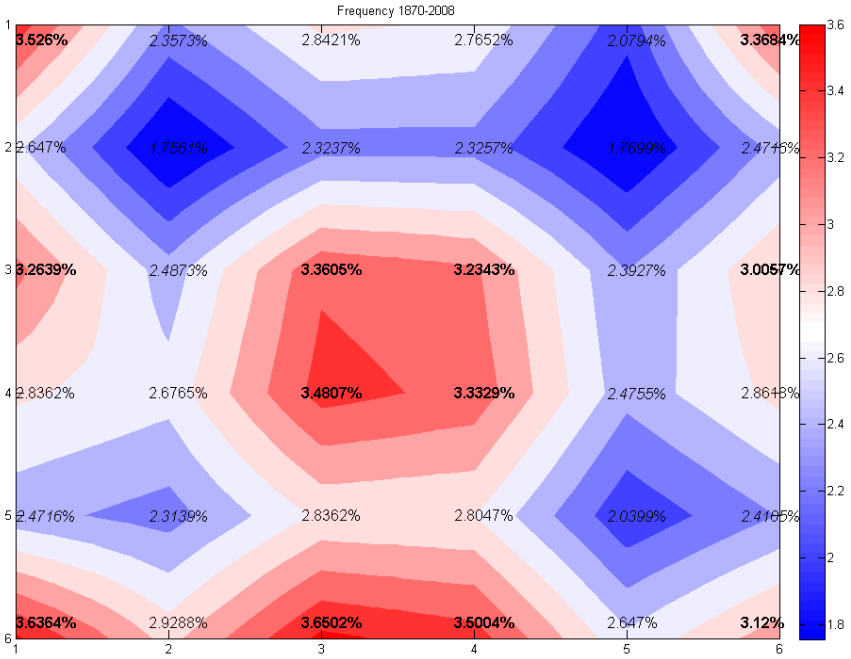

Fig. 21 Node frequency for 1870 to 2008 SLP SOM. Percentage numbers at coordinates show frequency of corresponding node in the Mater SOM. Percentage numbers of significantly high frequency nodes are bolded, while that of significantly low frequency nodes are italicized.

Bibliography

Abdalati, W. and K. Steffen, 2009: Snowmelt on the Greenland Ice Sheet as Derived from Passive Microwave Satellite Data. *J. Climate,* **10**, Issue 2, Pp.165-175.

Alley, R. B., E. S. Saltzman, K. M. Cuffey, and J. J. Fitzpatrick, 1990: Summertime Formation of Depth Hoar in Central Greenland. *Geophys. Res. Lett.*, **17**(12):2393–2396.

Alley, R. B. and coauthors, 2007: Observations: Changes in Snow, Ice and Frozen Ground. *Climate Change 2007: The Physical Science Basis,* P. Lemke et al., Eds., Cambridge Univ. Press, Cambridge, 361–368.

Anklin, M., R. C. Bales, E. Mosley-Thompson, and K. Steffen, 1998: Annual Accumulation at Two Sites in Northwest Greenland during Recent Centuries, *J. Geophys. Res.*, **103**(D22), 28,775–28,783, Doi:10.1029/98JD02718.

Appenzeller, C., J. Schwander, S. Sommer, and T. F. Stocker, 1998: The North Atlantic Oscillation and its Imprint on Precipitation and Ice Accumulation in Greenland, *Geophys. Res. Lett.*, **25**(11), 1939–1942, Doi:10.1029/98GL01227.

Bales, R. C., J. R. Mcconnell, E. Mosley-Thompson, and B. Csatho, 2001: Accumulation Over the Greenland Ice Sheet from Historical and Recent Records, *J. Geophys. Res.*, **106**(D24), 33,813–33,825, Doi:10.1029/2001JD900153.

Bamber, J., S. Layberry, and S. Gogineni, 2001: A New Ice Thickness and Bed Data Set for the Greenland Ice Sheet. 1: Measurement, Data Reduction, and Errors. *J. Geophys. Res.*, **106**, 33 773-33 780.

Banta, J. R., and J. R. Mcconnell 2007: Annual Accumulation over Recent Centuries at Four Sites in Central Greenland, *J. Geophys. Res.*, **112**, D10114, Doi:10.1029/2006JD007887.

Box, J. E., D. H. Bromwich, and L.-S. Bai, 2004: Greenland Ice Sheet Surface Mass Balance 1991–2000: Application of Polar MM5 Mesoscale Model and In Situ Data, *J. Geophys. Res.*, **109**, D16105, doi:10.1029/2003JD004451.

Box, J. E., L. Yang, J. Rogers, D. Bromwich, L.-S. Bai, K. Steffen, J. Stroeve, and S.-H. Wang, 2005: Extreme Precipitation Events over Greenland: Consequences to Ice Sheet Mass Balance, paper 5.2 presented at 8th International Conference on Polar Meteorology and Oceanography, *Am. Meteorol. Soc.*, San Diego, Calif., 9–13 Jan.

Box, J. E., D. H. Bromwich, B. A. Veenhuis, L.-S. Bai, J. C. Stroeve, J. C. Rogers, K. Steffen, T. Haran, and S.-H. Wang, 2006: Greenland Ice Sheet surface mass balance variability (1988–2004) from calibrated Polar MM5 output, *J. Clim.*, **19(**12), 2783–2800, doi:10.1175/JCLI3738.1.

Box, J. E., L. Yang, D. H. Bromwich, and L.-S. Bai, 2009: Greenland Ice Sheet Surface Air Temperature Variability: 1840–2007*. *J. Clim.*, **22**, 4029–4049. Doi: 10.1175/2009JCLI2816.1

Benson, C. S., 1962: Stratigraphic Studies in the Snow and Firn of the Greenland Ice Sheet, *Res. Rep. A245733*, U.S. Snow, Ice, and Permafrost, *Res. Estab.*, Wilmette, Ill.

Bromwich, D. H., R. I. Cullather, Q. Chen, and B. M. Csatho, 1998: Evaluation of Recent Precipitation Studies for Greenland Ice Sheet. *J. Geophys. Res.*, **103**, 26 007–26 024.

Bromwich, D. H., Q. Chen, Y. Li, and R. I. Cullather, 1999: Precipitation over Greenland and its Relation to the North Atlantic Oscillation, *J. Geophys. Res.*, **104**(D18), 22,103–22,115, Doi:10.1029/1999JD900373.

Burgess, E. W., R. R. Forster, J. E. Box, E. Mosley-Thompson, D. H. Bromwich, R. C. Bales, and L. C. Smith, 2010: A Spatially Calibrated Model of Annual Accumulation Rate on the Greenland Ice Sheet (1958–2007), *J. Geophys. Res.*, **115**, F02004, Doi:10.1029/2009JF001293.

Calanca, P., H. Gilgen, S. Ekholm, and A. Ohmura, 2000: Gridded Temperature and Accumulation Distributions for Greenland for Use in Cryospheric Models, *Ann. Glaciol.*, **31**, 118–120, doi:10.3189/172756400781820345.

Carse, J. C., D. Braaten, C. Laird, A. Gilbreath, and M. Oswald, 2010: An Accuracy Assessment of the Polar MM5 Model of Annual Snow Accumulation on the Greenland Ice Sheet.

Cavazos, T., 1999: Large-scale Circulation Anomalies Conducive to Extreme Precipitation Events and Derivation of Daily Rainfall in Northeastern Mexico and Southeastern Texas. *J. Clim.*, **12**, 1506–1523.

Cavazos, T., 2000: Using Self-Organizing Maps to Investigate Extreme Climate Events: an Application to Wintertime Precipitation in the Balkans. *J. Clim.*, **13**, 1718–1732.

Chen, Q.-S., D. H. Bromwich, and L.-S. Bai, 1997: Precipitation over Greenland Retrieved By a Dynamic Method and its Relation to Cyclonic Activity*. *J. Climate*, **10**, 839–870.Doi: 10.1175/1520-0442(1997)010<0839:POGRBA>2.0.CO;2

Church, J. A., J. M. Gregory, P. Huybrechts, M. Kuhn, K. Lambeck, M. Nhuan, D. Qin, and P. Woodworth, 2001: Changes in Sea Level, *Climate Change 2001: The Scientific Basis*, J. T. Houghton Et Al., Eds., Cambridge Univ. Press, Cambridge , 639– 693.

Compo, G.P., J.S. Whitaker., P.D. Sardeshmukh, N. Matsui, R.J. Allan, X. Yin, B.E. Gleason Jr., R.S. Vose, G. Rutledge, P. Bessemoulin, S. Bro¨Nnimann, M. Brunet, R.I. Crouthamel, A.N. Grant, P.Y. Groisman, P.D. Jones, M.C. Kruk, A.C. Kruger, G.J., Marshall, M. Maugeri, H.Y. Mok, Ø. Nordl, T.F. Ross, R.M. Trigo, X.L. Wang, S.D. Woodruff, and S.J. Worley. 2011: The Twentieth Century Reanalysis Project. *Q. J. R.*

Dethloff, K., M. Schwager, J. H. Christensen, S. Kiilsholm, A. Rinke, W. Dorn, F. Jung-Rothenhäusler, H. Fischer, S. Kipfstuhl, and H. Miller, 2002: Recent Greenland Accumulation Estimated from Regional Climate Model Simulations and Ice Core Analysis, *J. Clim.*, **15**(19), 2821–2832, doi:10.1175/15200442(2002)015<2821-:RGAEFR>2.0.CO;2.

Dibb, J. E. and M. Fahnestock, 2004: Snow Accumulation, Surface Height Change, and Firn Densification at Summit, Greenland: Insights from 2 Years of In Situ Observation. *J. Geophys. Res.*, **109**, D24113, doi:10.1029/2003JD004300.

Ettema, J., M. R. van den Broeke, E. van Meijgaard, W. J. van de Berg, J. L. Bamber, J. E. Box, and R. C. Bales, 2009: Higher Surface Mass Balance of the Greenland Ice Sheet Revealed by High-Resolution Climate Modeling, *Geophys. Res. Lett.*, **36**, L12501, doi:10.1029/2009GL038110.

Fahnestock, M., R. Bindschadler, R. Kwok, and R. Jezek, 1993: Greenland Ice Sheet Surface Properties and Ice Dynamics from ERS-1 SAR Imagery, *Science*, **262**, No. 5139, Pp.1530-1534.

Feldstein, S. B., and C. Franzke, 2006: Are the North Atlantic Oscillation and the Northern Annular Mode distinguishable? *J. Atmos. Sci.*, **63**, 2915-2930.

Fettweis, X., E. Hanna, H. Gallée, P. Huybrechts, and M. Erpicum, 2008: Estimation of the Greenland Ice Sheet Surface Mass Balance for the 20th and 21st Centuries, *Cryosphere*, **2**, 117–129.

Glover, R. W., 1999: Influence of Spatial Resolution and Treatment of Orography on GCM Estimates of the Surface Mass Balance of the Greenland Ice Sheet, *J. Clim.*, **12**(2), 551–563, doi:10.1175/1520-0442(1999)012<0551:IOSRAT>2.0.CO;2.

Hall, A. and X. Qu, 2006: Using the Current Seasonal Cycle to Constrain Snow Albedo Feedback in Future Climate Change, *Geophys. Res. Lett.*, 33, L03502, Doi:10.1029/2005GL025127.

Hanna, E., P. Huybrechts, I. Janssens, J. Cappelen, K. Steffen, and A. Stephens, 2005: Runoff and Mass Balance of the Greenland Ice Sheet: 1958–2003, *J. Geophys. Res.*, **110**, D13108, doi:10.1029/2004JD005641.

Hanna, E., A. Stephens, J. McConnell, S. Das, and J. Cappelen, 2006: Observed and Modeled Greenland Ice Sheet Snow Accumulation, 1958–2003, and Links with Regional Climate Forcing, *J. Clim.*, **19**(3), 344–358, doi:10.1175/JCLI3615.1.

Hanna, E., P. Huybrechts, K. Steffen, J. Cappelen, R. Huff, C. Shuman, T. Irvine-Fynn, S. Wise, and M. Griffiths, 2008: Increased Runoff from Melt from the Greenland Ice Sheet: A Response to Global Warming. *J. Climate*, **21**, 331–341. Doi:10.1175/2007JCLI1964.1

Harley, D. G., 1960: Frontal Contour Analysis of a 'Polar Low'. *Meteorol. Mag.*, **89**, 146–147.

Harrold, T. W. and K. A. Browning, 1969: Polar Low as a Baroclinic Disturbance. *Q. J. R. Meteorol. Soc.*, **95**, 710–723.

Hassol, S.J., 2004: Arctic Climate Impact Assessment, Impacts of a Warming Arctic. Cambridge Univ. Press, Cambridge.

Hansen, J., R. Ruedy, M. Sato, and K. Lo, 2010: Global Surface Temperature Change, *Rev. Geophys.*, **48**, RG4004, Doi:10.1029/2010RG000345.

Hewitson, B C, and R. G. Crane. 2002: Self-Organizing Maps: Applications to Synoptic Climatology. *Climate Res.*,**22**, No. 1: 13-26.

Hurrell, J. W. 1995: Decadal Trends in the North Atlantic Oscillation: Regional Temperatures and Precipitation, *Science*, **269**, 676– 679.

Hurrell, J.W., Y. Kushnir, G. Ottersen, and M. Visbeck, 2003: The North Atlantic Oscillation: Climate Significance and Environmental Impact, *Eds. Geoph. Monog. Series*, **134**, 279pp.

Hurrell, J.W., James W, and Clara Deser. 2009: North Atlantic Climate Variability: The Role of the North Atlantic Oscillation. *J. Marine Syst.*, **78**, 28-41.,Doi:10.1016/J.Jmarsys.2008.11.026.

Hutterli, M. A., C. C. Raible, and T. F. Stocker, 2005: Reconstructing Climate Variability from Greenland Ice Sheet Accumulation: An ERA40 Study, *Geophys. Res. Lett.*,**32**, L23712, Doi:10.1029/2005GL024745.

IPCC, 2007: Climate Change 2007: Impacts, Adaptation and Vulnerability. *Cambridge Univ. Press, Cambridge.*

Johannessen, O. M., K. Khvorostovsky, M. W. Miles, and L. P. Bobylev, 2005: Recent Ice-Sheet Growth in the Interior of Greenland, *Science*, **310**, No.5750 Pp.1013-1016, Doi: 10.1126/Science.1115356.

Kohonen, T., 1989: Self-organization and Associative Memory, 3rd edn., *Springer-Verlag*, Berlin

Kohonen, T., 1990: The Self-Organizing Map. *Proc. IEEE*, **78**(9): 1464–1480

Kohonen, T., 1995: Self-Organizing Maps. *Springer-Verlag*, Heidelberg.

Kristjansson, J. E. and H. McInnes, 1999: The Impact of Greenland on Cyclone Evolution in the North Atlantic. *Quart. J. Roy. Meteor. Soc.*, **125**, 2819–2834.

Lemke, P., J. Ren, R.B. Alley, I. Allison, J. Carrasco, G. Flato, Y. Fujii, G. Kaser, P. Mote, R.H. Thomas and T. Zhang, 2007: Observations: Changes In Snow, Ice And Frozen Ground. In: *Climate Change 2007: The Physical Science Basis. Contribution Of Working Group I To The Fourth Assessment Report Of The Intergovernmental Panel On Climate Change* [Solomon, S., D. Qin, M. Manning, Z. Chen, M. Marquis, K.B. Averyt, M. Tignor And H.L. Miller (Eds.)]. *Cambridge Univ. Press, Cambridge*.

Mailhot, J., D. Hanley, B. Bilodeau and O. Hertzman, 1996: A Numerical Case Study of a Polar Low in the Labrador Sea. *Tellus A*, **48A**, 383–402.

Main, J.P.L., 1997: Seasonality of Circulation in Southern Africa Using the Kohonen Self-Organizing Map. MSc thesis, University of Cape Town

Malmgren, B.A. and A. Winter, 1999: Climate Zonation in Puerto Rico Based on Principal Components Analysis and an Artificial Neural Network. *J. Clim.*, **12**, 977–985.

Mcconnell, J. R., R. C. Bales, D. Belle-Oudry, J. D. Kyne, G. Lamorey, E. Hanna, and E. Mosley-Thompson, 2001: Annual Net Snow Accumulation Over Southern Greenland From 1975 To 1998, *J. Geophys. Res.*, **106**(D24), 33,827–33,837, Doi:10.1029/2001JD900129.

Moore, G. W. K., M. C. Reader, J. York and S. Sathiyamoorthy, 1996: Polar Lows in the Labrador Sea – A Case Study. *Tellus A*, **48A**, 17–40.

Moore, G.W. K. and P.W. Vachon, 2002: A Polar Low over the Labrador Sea: Interactions with Topography and an Upper-level Potential Vorticity Anomaly, and an

Observation by RADARSAT-1 SAR. *Geophys. Res. Lett.*, **29**, 1773, DOI:10.1029/2001GL014007.

Murphy, B. F., I. Marsiat, and P. Valdes, 2002: Atmospheric Contributions to the Surface Mass Balance of Greenland in the HadAM3 Atmospheric Model, *J. Geophys. Res.*, **107**(D21), 4556, doi:10.1029/2001JD000389.

Mosley-Thompson, E., J. R. Mcconnell, R. C. Bales, Z. Li, P.-N. Lin, K. Steffen, L. G. Thompson, R. Edwards, and D. Bathke, 2001: Local to Regional-Scale Variability of Annual Net Accumulation on the Greenland Ice Sheet from PARCA Cores, *J. Geophys. Res.*, **106**, 33,839–33,851, Doi:10.1029/2001JD900067.

Mosley-Thompson, E., C. R. Readinger, P. Craigmile, L. G. Thompson, and C. A. Calder, 2005: Regional Sensitivity of Greenland Precipitation to NAO Variability, *Geophys. Res. Lett.*, **32**, L24707, Doi:10.1029/2005GL024776.

Mote, T. L. 1998: Mid-Tropospheric Circulation and Surface Melt on the Greenland Ice Sheet. Part I: Atmospheric Teleconnections. *Int. J.Climatol.*, **18**, 111–129. Doi: 10.1002/(SICI)1097-0088(199802)18:2<111::AID-JOC227>3.0.CO;2-X

Mote, T. L. 2007: Greenland Surface Melt Trends 1973–2007: Evidence of a Large Increase in 2007, *Geophys. Res. Lett.*, **34**, L22507, Doi:10.1029/2007GL031976.

Ohmura, A., and N. Reeh, 1991: New Precipitation and Accumulation Maps of Greenland, *J. Glaciol.*, **37**, 140–148.

Ohmura, A., M. Wild, and L. Bengtsson, 1996: A Possible Change in Mass Balance of Greenland and Antarctica in the Coming Century, *J. Clim.*, **9**(9), 2124–2135, Doi:10.1175/1520-0442(1996)009<2124:APCIMB>2.0.CO;2.

Ohmura, A., P. Calanca, M. Wild, and M. Anklin, 1999: Precipitation, Accumulation and Mass Balance of the Greenland Ice Sheet, *Z. Gletscherkd. Glazialgeol.*, **35**, 1–20.

Petersen, G. N., H. Olafsson, and J. E. Kristjansson, 2003: Flow in the Lee of Idealized Mountains and Greenland. *J. Atmos. Sci.,* **60**, 2183–2195.

Polyakova, E. I., A. G. Journel, I. V. Polyakov, and U. S. Bhatt, 2006: Changing Relationship Between the North Atlantic Oscillation and Key North Atlantic Climate Parameters. *Geophys. Res. Lett*, **33**, L03711.

Rasmussen, E. A. and J. Turner, 2003: Polar Lows: Mesoscale Weather Systems in the Polar Regions, 1st Edition. *Cambridge Univ. Press, Cambridge*, pp. 612.

Rink, T.P., 2006: Design and Evaluation of a Fine-Resolution Radar for Mapping Near-Surface Layers Using Plane-Waves. MSc thesis, Center for Remote Sensing of Ice Sheets, University of Kansas.

Rogers, J. C., and H. Van Loon, 1979: The Seesaw in Winter Temperatures between Greenland and Northern Europe. Part II: Some Oceanic and Atmospheric Effects in Middle and High Latitudes. *Mon. Wea. Rev.*, **107**, 509–519. Doi: 10.1175/1520-0493(1979)107<0509:TSIWTB>2.0.CO;2

Rogers, J. C., and M. J. McHugh, 2002: On the Separability of the North Atlantic Oscillation and Arctic Oscillation. *Climate Dyn.,* **19,** 599–608.

Schuenemann, K. C., J. J. Cassano, J. Finnis, 2009: Synoptic Forcing of Precipitation over Greenland: Climatology For 1961–99. *J. Hydrometeor*, **10**, 60–78. Doi: 10.1175/2008JHM1014.1.

Snow, Water, Ice and Permafrost in the Arctic (SWIPA), 2009: Summary – the Greenland Ice Sheet in a Changing Climate

Slutz, R.J., S.J. Lubker, J.D. Hiscox, S.D. Woodruff, R.L. Jenne, D.H. Joseph, P.M. Steurer, and J.D. Elms, 1985: Comprehensive Ocean-Atmosphere Data Set; Release 1. NOAA Environmental Research Laboratories, Climate Research Program, Boulder, CO, 268 pp. (NTIS PB86-105723)

Tibshirani, R., G. Walther, and T. Hastie, 2001: Estimating the Number of Clusters in a Data Set via the Gap Statistic. *J. R. Stat. Soc.: Series B (Statistical Methodology)*, **63**(2), 411-423.

Thomas, R., E. Frederick, W. Krabill, S. Manizade, and C. Martin, 2006: Progressive Increase in Ice Loss from Greenland, *Geophys. Res. Lett.*, **33**, L10503, Doi:10.1029/2006GL026075.

Thompson, S. L., and D. Pollard, 1997: Greenland and Antarctic Mass Balances for Present and Doubled Atmospheric CO2 from the GENESIS Version-2 Global Climate Model, *J. Clim.*, **10**(5), 871–900, Doi:10.1175/15200442(1997)010<0871:-GAAMBF>2.0.CO;2.

Tsukernik, M., D. Kindig, and M. C. Serreze, 2007: Characteristics of Winter Cyclone Activity in the Northern North Atlantic: Insights from Observations and Regional Modeling. *J. Geo- phys. Res.*, **112**, D03101, doi:1029/2006JD007184.

Vinther, B. M., K. K. Andersen, P. D. Jones, K. R. Briffa, and J. Cappelen (2006), Extending Greenland Temperature Records into the Late Eighteenth Century, *J. Geophys. Res.*, **111**, D11105, Doi:10.1029/2005JD006810.

Woodruff, S. D., S. J. Worley, S. J. Lubker, Z. Ji, J. Eric Freeman, D. I. Berry, P. Brohan, E. C. Kent, R. W. Reynolds, S. R. Smith, and C. Wilkinson, 2011: ICOADS Release 2.5: Extensions and Enhancements to the Surface Marine Meteorological Archive. *Int. J. Climatol.*, **31**: 951–967. doi: 10.1002/joc.2103